

COUPLED CHANNEL–FLOODPLAIN DYNAMICS AND RESULTING STRATIGRAPHIC ARCHITECTURE VIEWED THROUGH A MASS-BALANCE LENS

KYLE M. STRAUB,¹ RIPUL DUTT,¹ AND ROBERT A. DULLER²

¹Department of Earth and Environmental Sciences, Tulane University, New Orleans, Louisiana 70118, U.S.A.

²Department of Earth, Ocean and Ecological Sciences, University of Liverpool, Liverpool L69 3BX, U.K.

email: kmstraub@tulane.edu

ABSTRACT: Basin-wide accommodation production and associated sediment mass deposition exert fundamental controls on stratigraphic architecture, but the details of this relationship are not fully understood. This is because it is unknown how accommodation production directly influences morphodynamics both in terms of channel process (i.e., channel migration, channel avulsion) and floodplain process, both of which are themselves coupled dynamically and are critical to the nature of stratigraphic architecture. To address this, we expand on existing theory that links sediment mass balance and resultant stratigraphic architecture. We use two fan-delta experiments that each experience different rates of accommodation production to measure key surface morphometrics and subsurface sedimentary characteristics. Importantly, sediment was transported in bedload and suspension in these experiments, resulting in construction of strata characterized by channel bodies surrounded by overbank strata deposited from suspension fallout. From these data we use three key timescales to capture the overall behavior of the system when placed into mass-balance space: avulsion setup timescales (T_A) and channel mobility timescales (T_V) that define short-term surface autogenics, and an accretion timescale (T_C) that incorporates longer-term deposition. We find that the ratio of both T_C/T_A and T_C/T_V are independent of accommodation production rate in mass-balance space, which supports a self-organized response of channel dynamics to environmental boundary conditions. The fraction of strata generated from key depositional environments largely supports this behavior, particularly for channel sand bodies that resulted in deposition from bedload transport. As such, our results suggest that channel-body density is independent of accommodation production rate in a mass-balance space. We found that, although contributing to a significant fraction of the basin strata, far-field overbank deposition rates are insensitive to accommodation production and that differences in autogenic timescales between experiments largely resulted from differences in channel deposition rates, highlighting the close coupling between channel dynamics and accommodation generation. More generally the observed self-organized response of surface morphodynamics to accommodation production in mass-balance space provides a process-based framework to explain the utility of balancing mass for the prediction of down-system sediment size fractionation and sedimentary architecture.

INTRODUCTION

The spatial arrangement of channel bodies, encased within floodplain strata, is often referred to as alluvial stratigraphic architecture (e.g., Allen 1978; Leeder 1978; Bridge and Leeder 1979; Kraus 2002; Hickson et al. 2005; Wang et al. 2021) (Fig. 1). Primary controls on this architecture include the depth and width of channels (Bristow and Best 1993) as well as their lateral migration and avulsion rates (Bryant et al. 1995; Jerolmack and Mohrig 2007; Jerolmack and Paola 2007; Hajek 2009; Hajek et al. 2010). Thus, environmental forcings that influence channel geometry and mobility have the potential to be recorded in alluvial stratigraphic architecture. While relationships between some forcings and stratigraphic architecture have been explored, including the character of hydrographs (Plink-Björklund 2015; Esposito et al. 2018; Barefoot et al. 2021) and sediment properties (Tomqvist 1993; Caldwell and Edmonds 2014; Hariharan et al. 2021), much of what we know about stratigraphic architecture concerns channel-centric processes. However, a renewed

appreciation of the co-evolution of channels and their floodplains can be seen in several recent studies (Hajek 2015; Esposito et al. 2018; Barefoot et al. 2021; Martin and Edmonds 2021; Chamberlin and David et al. 2022; Han and Kim 2022). We follow a definition of floodplains as the relatively flat topographic surfaces adjacent to rivers that experience inundation on annual to decadal timescales, and can be distinguished from regions that are not regularly inundated (Sutfin et al. 2016).

Quantitative exploration of stratigraphic architecture has its roots in a series of publications that modeled the aggradation of individual strike-oriented sections of alluvial strata (Allen 1978; Leeder 1978, Bridge and Leeder 1979). Following commonly used nomenclature, we refer to these as the LAB models. Inspired by these early studies, similar models are still in use today (Chamberlin and Hajek 2015, 2019; Chamberlin et al. 2016). Under a constant rate of tectonic subsidence, river channels in the LAB models were prescribed to avulse at a set frequency and relocate to random positions in the basin. Deposition outside channels (overbank deposition)

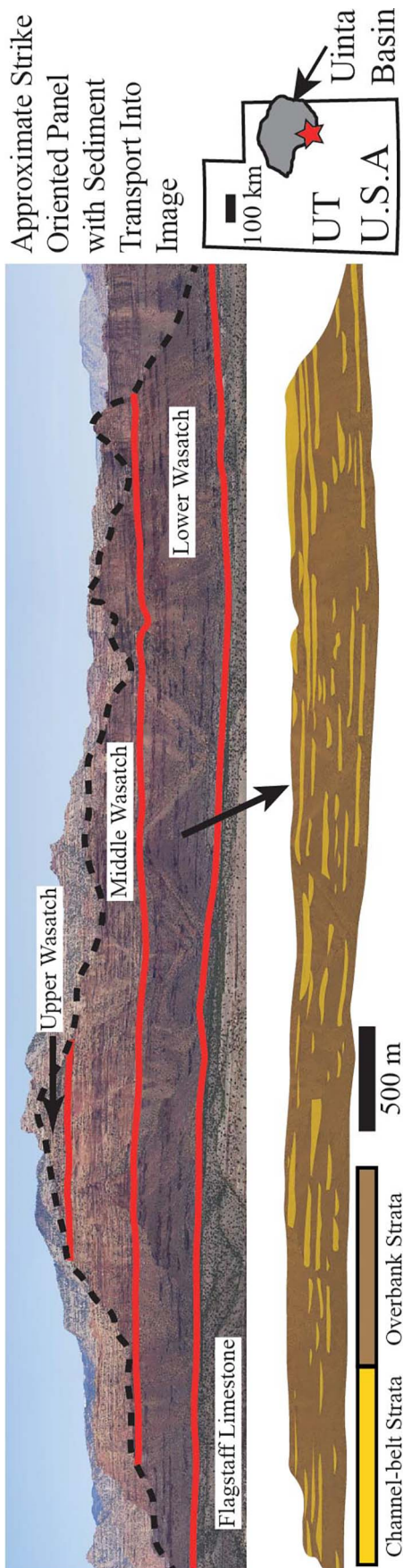


FIG. 1.—The lower Wasatch Formation as observed in the Uinta Basin, UT, U.S.A., exemplifies alluvial strata constructed in basins that preserve significant fractions of both channelized and overbank strata. Sediment transport direction is into the image. Image modified from Pisel et al. (2018) and provided courtesy of David Pyles. The lower panel represents interpretation of outcrop into channel bodies and overbank strata.

was modeled in the simplest fashion possible, prescribed as a uniform rate that did not vary in time or space. Relocation of channels through avulsion resulted in the removal of floodplain and replacement with channelized strata. While advances have been made in our understanding of overbank sedimentation since publication of the LAB models (Pizzuto 1987; Pizzuto et al. 2008; Toonen et al. 2017; Martin and Edmonds 2021), our knowledge of sedimentation processes in channels still far exceeds our understanding of floodplain deposition. This was highlighted in a study by Jerolmack and Paola (2007), who modeled the accumulation of fluvial strata. Given uncertainty in how to model overbank strata, they explored the consequences of different algorithms: uniform, elevation dependent, and noisy overbank deposition. The choice of algorithm implemented had important implications for the spatial arrangement of sand bodies in the strata. While advances in our understanding of overbank sedimentation have occurred since the Jerolmack and Paola (2007) modeling work, we still lack process theory for overbank sedimentation that rivals the sophistication of our theory for channels.

Exploration of processes that produce fluvial stratigraphic architecture has been stifled by the difficulty in producing fluvial landscapes at laboratory scale that construct strata from both bedload-dominated channelized processes and suspension-fallout deposition in overbank settings. Almost all physical experiments that explore construction of channelized strata are associated with transport systems that move sediment near exclusively in bedload (Wood et al. 1993; Strong et al. 2005; Swenson 2006; Wang et al. 2011; Muto and Powell et al. 2012; Ganti et al. 2019). However, a sediment mixture developed by Hoyal and Sheets (2009) does generate landscapes and strata by a mixture of bed-load and suspended-load transport, with overbank strata resulting from suspension fallout. Here, we use a similar mixture to explore the control of accommodation generation on the architecture of fluvial–deltaic strata.

The space made available to store sediment is termed accommodation and is primarily set by subsidence and sea-level rise rates. While accommodation is formally defined in a volumetric framework (Jervey 1988), we follow a definition that quantifies the vertical distance between the current Earth-surface and the long-term equilibrium topography at a point in space (Muto and Steel 2000). With this definition, we can define a rate of accommodation production with dimensions of L/T . A central goal of this work is to use physical experiments to develop a theoretical framework to quantify how accommodation production influences channel–floodplain processes (i.e., morphodynamics), and how this in turn influences alluvial sedimentary architecture.

Under a constant rate of tectonic subsidence river channels in the LAB models were prescribed to avulse at a set frequency and relocate to random positions in the basin. An early avenue of exploration focused on the rate of accommodation production for the density and interconnectedness of channel bodies in the subsurface. The LAB models predicted that accommodation production rate was inversely related to channel-body density in the resulting strata (Fig. 2B). However, physical experimental observations suggest that rates of channel avulsion are proportional to long-term sediment accumulation rates (Bryant et al. 1995; Chadwick et al. 2020). Here, we refer to long-term sediment accumulation rates as those measured over time-scales in which subsidence rates dictate sedimentation rates. These same experiments and other stratigraphic architecture models produce the opposite relationship between accommodation generation and preserved channel-body density found in the LAB models (Heller and Paola 1996). Further, a compilation of 20 published field studies found no consistent relationship between channel-body stacking density and long-term aggradation rates (Colombera et al. 2015).

A test of the LAB model predictions was undertaken in a physical experiment performed in the eXperimental Earth-Scape (XES) facility in 1999 (Hickson et al. 2005; Strong et al. 2005). This experiment included two stages that differed in their absolute subsidence rates. However, to keep the average shoreline location at an equal location, water and sediment feed

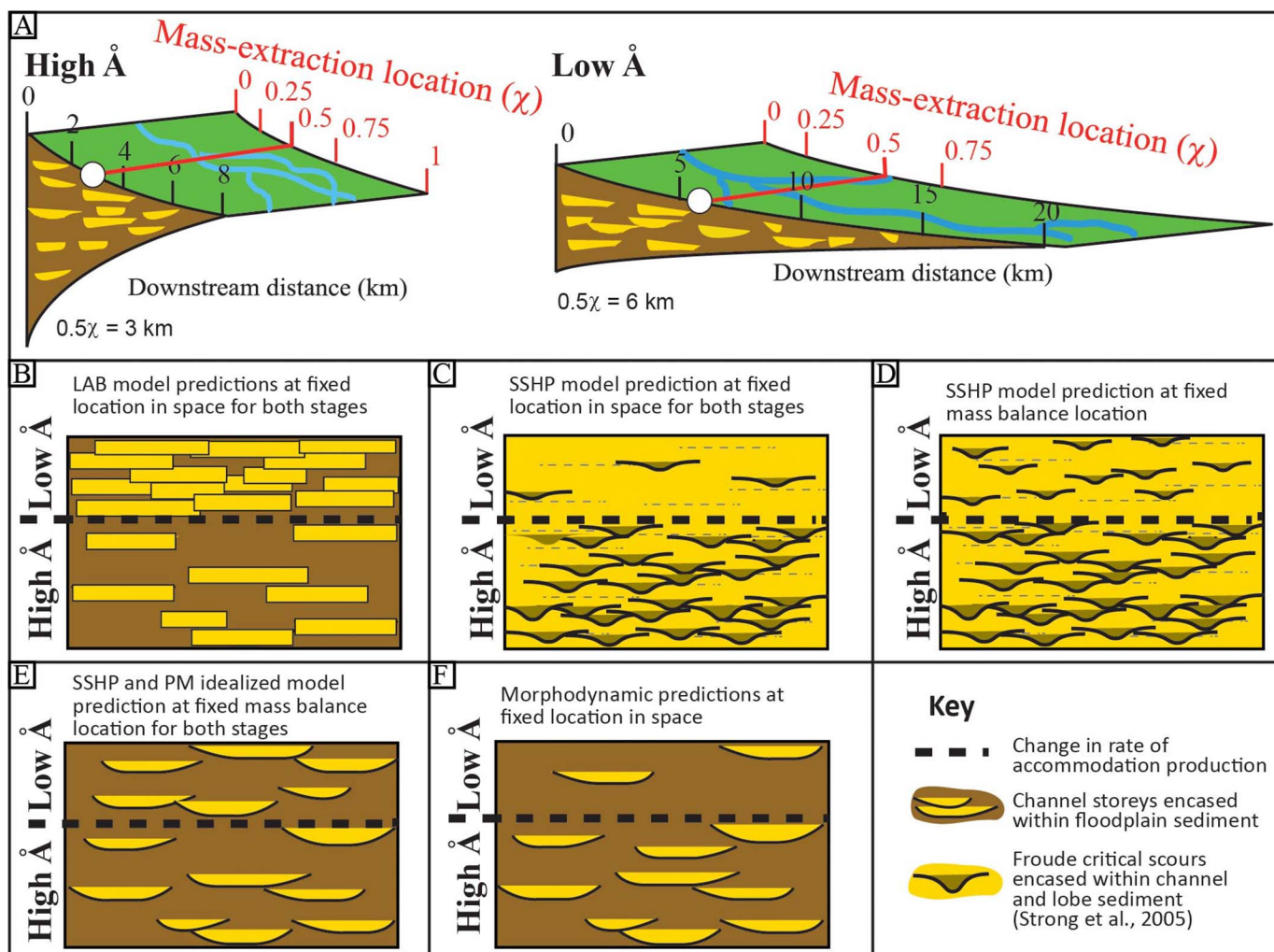


FIG. 2.—A) Schematic illustrating a segment of a sediment routing system with measurement of length as both a dimensional distance and dimensionless mass-extraction distance from an upstream segment boundary. B–F) Conceptual models of the influence of accommodation production rate on stratigraphic architecture and example stratigraphy that contains channel-belt deposits encased in overbank strata. In each conceptual model a step change separates older strata deposited in a high-accommodation production setting from younger strata constructed in a low-accommodation setting. B) Conceptual model generated from LAB publications. Along a vertical section of strata at a fixed location in space, the LAB models predict an increase in channel density with a decrease in accommodation production rate. C) Conceptual model of Strong et al. (2005), SSHP, findings where a decrease in channel scour density resulted from a decrease in accommodation production at a fixed location in space. D) Placing the strata of the SSHP study in a mass-extraction framework removed most, but not all, the differences in channel scour density between the two stages. E) An idealized model of SSHP and Paola and Martin (2012), PM, suggest similar density of channel bodies encased in floodplain strata if placed in a mass-extraction framework. F) This same strata, if viewed at a fixed location in space, would show a reduction in channel-body density with reduction in accommodation production rate.

rates also differed between the experimental stages. The switch in forcing parameters between stages induced a change in transport slope, which resulted in deposits of differing length and so were not directly comparable in terms of their sedimentary architecture. To account for this, Strong et al. (2005) developed a mass-balance transformation for sedimentary basins. This transformation converts a distance from a basin inlet to a dimensionless parameter equal to the ratio of the sediment mass deposited upstream of a location of interest to the sediment mass deposited in the entire basin (Fig 2A). They applied this transformation to the strata of their two experimental stages, comparing architecture at equivalent mass-balance locations. Lacking channel-belts encased in floodplain strata, they mapped channel scour bodies in the strata that resulted from hydraulic jumps. These scour bodies were surrounded by other bedload deposits, including those resulting from channels and lobes. The mass-balance transformation removed much of the difference in stratigraphic architecture (Fig. 2C, D) observed in cross-sections of the two stages. However, some differences remained, including a higher scour body density

in the experimental stage with high subsidence rates, which they suggested might just be due to the higher input rates of water and sediment in this stage. A key finding of their study and a companion study (Paola and Martin 2012) though, was the importance of mass-extraction to stratigraphic architecture, which the authors suggested might be as important as previously explored parameters (Fig. 2E).

Here, we undertake an experimental campaign where only the production of accommodation is varied between two experiments that utilize a sediment mixture similar to that developed by Hoyal and Sheets (2009). We apply the mass-balance transformation to control for differences in the absolute planform dimensions of our experiments, thus allowing us to isolate the influence of accommodation production on channel–floodplain morphodynamics and the associated alluvial sedimentary architecture.

Our goal is to link mass-extraction to Earth-surface dynamics (morphodynamics) and stratigraphic architecture by exploring critical timescales that quantify the lateral mobility of fluvial networks and the vertical accumulation

of alluvial strata. Further, we explore the sensitivity of both channels and floodplains to accommodation production. For basins experiencing constant environmental conditions, processes internal to the sediment routing system (i.e., autogenic processes) control stratigraphic architecture over the timescales explored in stratigraphic architecture models (Sheets et al. 2002; Strong et al. 2005; Hajek and Straub 2017). Methods that quantify the timescales of these processes provide means to quantitatively compare the lateral and vertical dynamics of systems in a mass-balance framework. We suggest that timescale ratios that compare lateral to vertical dynamics correlate to stratigraphic attributes, including the density of preserved channel bodies and the volume of preserved overbank strata.

THEORY

Timescales of Channel Migration

Channels move over alluvial basins through slow lateral migration and punctuated relocation events, known as avulsions. A commonly used metric to assess the likelihood of river avulsion is the superelevation ratio. This parameter is defined as the relief between a levee crest and the elevation of the far-field floodplain normalized by the channel depth (Mohrig et al. 2000; Martin et al. 2009; Hajek and Wolinsky 2012), with rivers primed for avulsion when this ratio is order 1. This theory can be used to estimate a time between avulsions, T_A , as

$$T_A = \frac{H}{D_C - D_{FP}} \quad (1)$$

where H is a characteristic channel depth, D_C is a channel deposition rate, and D_{FP} is the far-field floodplain deposition rate (Jerolmack and Mohrig 2007), both measured over the timescale between avulsions. In this framework, deposition in both channels and floodplains impacts avulsion frequency.

On timescales longer than T_A , the mobility of channels leads to the reworking of sediments in the active layer (within ~ 1 channel depth of the surface) and deposition of channel sand geobodies. This channel mobility impacts the distribution of channel sand geobodies and the rate, timing, and preservation of floodplain deposits (Fielding et al. 2006; Martin et al. 2009; Kim et al. 2010; Wickert et al. 2013; Sahoo et al. 2020). Tracking the time necessary for a significant fraction of the terrestrial delta-top to experience surface modification by channelized flow allows a visitation timescale, T_V , to be calculated. This captures modification from both slow migration of channels and their punctuated relocation following avulsion. The average of the decay curves representing the change in fraction of unmodified area (f_{UM}) with timescale of observation follows an exponential decay:

$$f_{UM} = ae^{-bt} \quad (2)$$

where a and b are parameters dependent on boundary conditions, such as the rate of accommodation production, input grain-size distribution, sediment cohesion, vegetation, and hydrograph variability (Wickert et al. 2013; Straub et al. 2015; Li et al. 2017; Esposito et al. 2018; Barefoot et al. 2021). We define T_V as the time necessary to reduce f_{UM} to a near zero value, specifically 0.05 to avoid statistical irregularities that would be associated with tracking the time to f_{UM} reaching zero (Cazanacli et al. 2002; Wickert et al. 2013).

Timescales of Basin Filling

Next, we define a timescale that characterizes a vertical mobility, through deposition, of channelized systems. This is accomplished using the compensation timescale, T_C , which defines the time necessary for sedimentation to produce a deposit geometry that statistically matches the spatial (x, y) distribution of accommodation production in a basin (Sheets et al. 2002; Wang et al. 2011). This timescale is estimated by measuring a scale break in the decay of the standard deviation of deposition rates normalized by the long-

term accommodation production rate, σ_{SS} . This variability decays as a power-law function of the timescale of measurement, and the slope of this decay is termed the compensation index, κ (Straub et al. 2009). The value of κ indicates a style of basin filling, with higher values linked to a stronger statistical preference for deposition to occur in topographic lows, thus compensating topography. Over short timescales, in which autogenic processes influence the isopach of a related thickness of strata, κ_{ST} ranges between 0 to 1. However, over long timescales κ_{LT} is generally close to 1, indicating complete compensation and the one-to-one relationship between the spatial distribution of accommodation production in a basin and the isopach of a related thickness of strata. Here the subscripts ST and LT denote short and long timescale, respectively. Laboratory experiments suggest that T_C scales as the time necessary to generate a deposit with a mean basin-wide thickness equal to the maximum vertical roughness scale of the transport system (Sheets et al. 2002; Wang et al. 2011):

$$T_C \sim \frac{l}{D_{LT}} \quad (3)$$

In many systems l can be approximated as the maximum depth of channels at a given location in a basin and D_{LT} is the basin-wide long-term deposition rate. Given that some of the sediment associated with filling accommodation over a T_C timescale was deposited in a channel and some in a floodplain, we again highlight the dual importance of both depositional environments to critical morphodynamic and stratigraphic timescales.

Dimensionless Mobility Metrics

The long-timescale vertical to horizontal mobility of channelized sediment routing systems can be characterized by the ratio of T_C and T_V (e.g., Straub and Esposito 2013) to produce a dimensionless basin mobility index, T_{LT}^* :

$$T_{LT}^* = \frac{T_C}{T_V} \quad (4)$$

This ratio is similar to the channel mobility number proposed by Jerolmack and Mohrig (2007), but rather than characterizing mobility through the time necessary to aggrade a single channel by one channel depth and migrate that same channel by one channel width, we use parameters that characterize the longer-timescale evolution of a basin. Systems characterized by large T_{LT}^* have channels with high lateral mobility relative to long-term deposition rates and vice versa. We explore this parameter in mass-balance space to establish if the rate of accommodation production influences the relative ratio of vertical to horizontal system mobility and resulting gradients in stratigraphic products. We also construct a dimensionless variable to characterize the ratio of compensation and avulsion timescales:

$$T_{ST}^* = \frac{T_C}{T_A} \quad (5)$$

T_{ST}^* scales with the number of avulsions, which result in lateral movement of the channel network, that occur over a compensation timescale. We note that T_C and T_A are both impacted by deposition in channels and floodplains.

Constructing a Mass-Balance Framework

We explore gradients in surface process and stratigraphic timescales, and ratios of these timescales, within a mass-balance framework. This framework

is useful for conceptualizing controls on stratigraphic gradients, including the environment of deposition, in alluvial basins. We construct a mass-balance framework for our two experimental deposits using a slight modification of the method developed by Strong et al. (2005). They defined $\chi(x)$ as the ratio of sediment mass deposited between a source at $x = 0$ and a downstream distance, x , to the total mass of sediment deposited in the basin:

$$\chi(x) = \frac{\int_0^x D(x) dx}{\int_0^L D(x) dx} \quad (6)$$

where D is a rate of deposition and L is the total length of the system. Eq. 6 can be generalized for transport systems with variable width, B , and with knowledge of the total volumetric sediment supplied to a basin, $V_{s,0}$ (Paola and Martin 2012). Our framework is developed for single-channel-inlet basins that can bifurcate downstream of the basin inlet and migrate or avulse to fill accommodation. We emphasize that our results are specific to distributive systems and might vary in tributive systems (Weissmann et al. 2010). To account for the three-dimensional nature of many fan-deltas we utilize a radial distance, R , from the basin inlet, instead of x and account for porosity. This leads to the equation

$$\chi(R) = \frac{1}{V_{s,0}} \int_0^R B(R)D(R)\varepsilon_S(R)dR \quad (7)$$

where ε_S is the volumetric concentration of sediment in the deposit ($1 - \text{porosity}$).

The importance of mass-extraction on surface processes and stratigraphic architecture can partially be linked to systematic changes in the ratio of sediment to water. In some basins, specifically marginal marine systems, most water fluxes through channels and the landscapes that surround them until reaching the sea, with minimal loss to groundwater and evaporation (Winter 1999; Jasechko et al. 2021). As such, in these basins the ratio of sediment flux to water flux generally decreases with distance down system, which suggests that there should be systematic changes in channel aspect ratios and slopes (Parker et al. 1998; Whipple et al. 1998). Several studies highlight the importance of the ratio of sediment flux to water flux on channel morphodynamics (avulsion frequency and channel migration rates) (Bryant et al. 1995; Paola et al. 2001; Powell et al. 2012; Straub and Wang 2013; Wang et al. 2021). This ratio will change down-system, as sediment is deposited, which will initiate spatial gradients in fluvial morphodynamics and alluvial stratigraphic architecture. A mass-balance framework in essence normalizes these gradients for deposits of different absolute lengths, thus allowing their dynamics to be compared.

METHODS

Despite large differences in some governing dimensionless numbers, experimental and field-scale systems display scale independence and similarity in many deltaic morphodynamic metrics (Paola et al. 2009; Kleinhans et al. 2014). Here, we characterize the link between surface processes and stratigraphic architecture produced in two fan-delta experiments with significant sediment transport in suspension, some of which overtopped channel levees and was deposited in floodplains. These two experiments shared identical forcing, except for the rate of terrestrial accommodation production.

Experimental Setup

Experiments were conducted in a delta basin at the Tulane University Sediment Dynamics Laboratory. The dimensions of this basin are $4.2 \text{ m} \times 2.8 \text{ m} \times 0.65 \text{ m}$ (Fig. 3). We automate the rate of sediment (Q_S) and water (Q_W) delivery to the basin. In these experiments Q_S and Q_W were kept constant at $3.9 \times 10^{-4} \text{ kg/s}$ and $1.7 \times 10^{-4} \text{ m}^3/\text{s}$, respectively. Constant Q_S and Q_W are meant to simulate bankfull conditions, which typically occur for a few weeks every other year in natural systems (Williams 1978). Constant Q_S and Q_W values are a method to speed up time in experiments as most geomorphic work is thought to occur during these bankfull conditions. Sediment was released from a computer-controlled commercial feeder into a funnel where it mixed with water and was routed to the basin from an inlet channel, forming a fan-delta. Blue dye was added to input water to aid visualization of the flow field and characterization of deltaic morphodynamics. A weir on a computer-controlled vertical slide was in hydraulic communication with the basin and allowed for ocean elevation control with sub-millimeter precision.

Sediment delivered to the basin was modeled off the mixture developed by Hoyal and Sheets (2009), which is composed of particle sizes ranging from approximately $1 - 1000 \mu\text{m}$ with a mean of $67 \mu\text{m}$. Importantly, the sediment mixture included small amounts of bentonite, commercially available cat litter, and a granular polymer (New Drill Plus, distributed by Baker Hughes, Inc.). As discussed by Hoyal and Sheets (2009), when mixed with water these ingredients increase the cohesion of the experimental sediment surface. This increase in system cohesion allowed relatively narrow and deep channels to form from subcritical flows, which transported fine-grained sediment in suspension. To aid visualization of stratigraphic architecture, a quarter of the coarsest 23.5% of the distribution was commercially dyed red, while the remainder consisted of white particles.

The experiments begin with progradation of a delta into the basin with a constant base level of 25 mm. Progradation stages ceased when the resulting delta-top area matched a predicted area that combined with a planned base-level rise rate would generate terrestrial accommodation at a rate equivalent to the input volumetric sediment flux. This resulted in deltas whose shoreline location was in dynamic equilibrium with forcing conditions (Straub et al. 2015).

The main aggradation stage of an experiment began when sea-level rise was initiated. The aggradation stage for both experiments lasted 560 hours, and all data presented in this study comes from the aggradation stage. This duration was sufficient to generate tens of channel depths worth of stratigraphy. The only parameter that varied between experiments was the rate of accommodation production, \dot{A} . This choice facilitated the construction of two deltaic deposits with different mass-extraction profiles. The low \dot{A} experiment had a sea-level rise rate (r) of 0.1 mm/hr, while the high \dot{A} experiment had a sea-level rise rate of 0.25 mm/hr.

Data Collection

The primary data collected included topographic scans and co-registered images of the experimental surface. A FARO Focus3D-S 120 laser scanner was used to collect a point cloud of topography, which was converted to a digital elevation model (DEM) having grid spacing of 5 mm in the down-basin and cross-basin directions (thus cell area of 25 mm^2), and a vertical resolution of $< 1 \text{ mm}$ (Figs. 3, 4). Two scans were collected each run-hour. The first occurred near the end of the run-hour to capture an image of the flow field co-registered with topography. The second occurred after the end of each run-hour while the experiment was paused, yielding the highest-precision topography. As discussed in Straub et al. (2015), the temporal and spatial resolution of these scans is sufficient to characterize the mesoscale dynamics of the system, such as channel migration and channel and lobe avulsions.

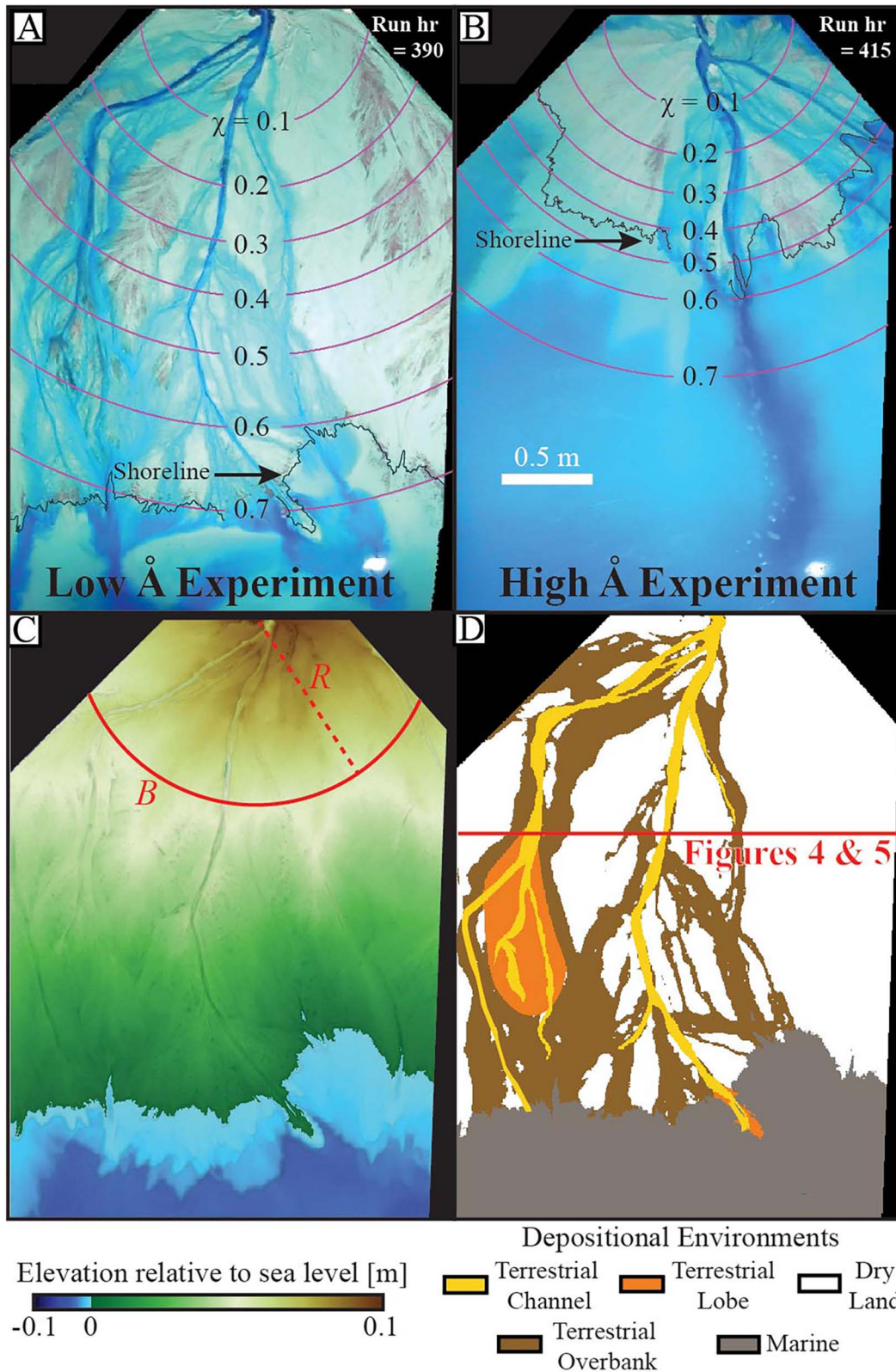


FIG. 3.—Characteristic images of the active experimental surface and depositional environments in the two experiments. **A, B**) Images of active experimental surfaces with flow dyed blue for the low- (run-hr 390) and high- (run-hr 415) \AA experiments, respectively. Purple lines denote contours of mass-extraction fractions, while black line denotes shoreline at that run-hour. **C**) Map of elevations relative to sea-level for run-hr 415 of the low- \AA experiment. Line B represents arc defined by radius R (dashed line). **D**) Map of depositional environments. Location of cross-sections presented in Figures 4 and 5 is shown in red.

After the active-run phase of the experiments ceased, cores were collected along a dip line at an interval of 0.5 m, starting at the entrance channel. Cores were dried and weighed to measure deposit porosity. Next, the deposits were sectioned along cross-basin transects with a spacing of 0.1 m.

Cross-sections were imaged using a Cannon G-10 camera and a laser scan. The visual color fields in the images were co-registered with the point cloud of the cross-section, resulting in undistorted and basin georeferenced images of the deposits.

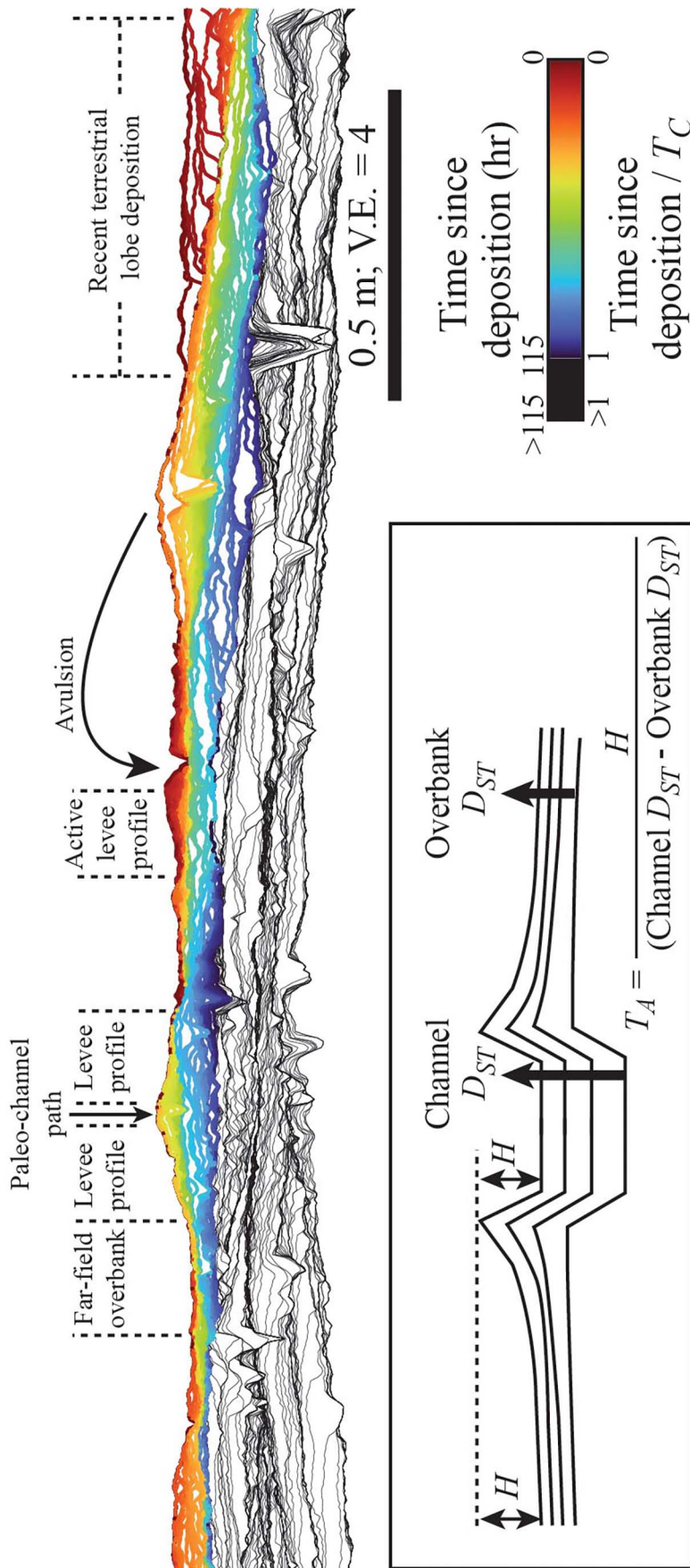


FIG. 4.—Synthetic stratigraphy produced during the first 390 hrs of the low- A experiment. Cross-section is oriented as if one is looking downstream, with location of cross-section noted in Figure 3D. Colored lines represent time since deposition normalized by the compensation timescale of the cross-section. Black lines represent surfaces deposited more than one compensation timescale before run-hour 390. Key depositional environments are noted. Inset shows schematic of key morphodynamic parameters necessary to estimate avulsion timescales.

Data Analysis

Measuring Morphodynamics.—We focus on measuring attributes important for characterizing timescales of autogenic surface dynamics in each experiment and linking these to the fraction of strata constructed in key depositional environments. Our first step is to generate maps of key depositional environments for each run-hour from co-registered maps of topography and digital images. We define five environments: terrestrial channels, terrestrial lobes, wet terrestrial overbank (floodplains), dry land, and marine (Fig. 3D). Terrestrial channels were mapped by hand using the FARO digital images. Channels were identified as linear flow features with relatively sharp blue intensity color gradients that separated channelized flow from overbank flow along levee crests. Channels often lost confinement before reaching the marine, resulting in deposition and construction of terminal terrestrial lobes. These lobes often migrated upstream due to morphodynamic backwater effects (Hoyal and Sheets 2009) until avulsions were triggered (Edmonds et al. 2009). The lateral extents of these lobes were also mapped by hand and identified by significant surface expressions of red (coarse) sand and lobate topography. In field scale systems, floodplains are defined as regions adjacent to channels that are occasionally inundated from flow that overtops channel levees (Sutfin et al. 2016). Given that our experiments are run with constant discharge, meant to simulate bankfull conditions, we characterize any terrestrial region that is inundated with flow and not a channel or a lobe as floodplain (here used interchangeably with overbank). Thus, active terrestrial floodplain environments were identified as cells above sea level and covered by active flow (identified by a blue intensity color threshold) that were not channels or lobes. The remaining terrestrial cells were registered as dry land. Finally, all cells located below sea level, defined for each run hour, were registered as marine. We highlight the range of depositional environments produced by the Hoyal and Sheets (2009) sediment mixture, which is greater than produced in bedload-dominated experiments.

Average profiles of down-delta topography are generated by taking all measurements of terrestrial topography, binning data based on radial distance from the entrance channel that are 5 mm wide, and averaging data in each bin. All parameters that are reported as a function of radial distance from the basin inlet are also measured at this 5 mm spacing. This data is then used to generate profiles of down-delta slope by differing topography at neighboring bins and dividing by the bin spacing. Given sensitivity of slope data to small-scale variations in average topography at the tight bin spacing, we apply a 0.1 m moving average to the slope data.

We measure the average number of channels as a function of distance from the basin inlet, as we recognize that T_V is influenced by both the number of channels on a surface and their mobility. A similar T_V value can be obtained by relatively few channels moving rapidly across a surface or by many channels moving slowly. However, these two situations would produce markedly different stratigraphic architecture.

Using channel maps and co-registered topography (Fig. 3), we estimate statistics of channel depths and widths as a function of distance from the basin inlet, as well as bulk statistics for the full routing system. For each channel identified along radial strike-sections, we subtract the minimum elevation present for a channel thread (approximating the thalweg) from the maximum elevation (approximating the levee crest). Channel widths are measured as the distance across radial transects between the start and end of channelized flow. This assumes that channels are flowing perpendicular to the radial cross-section, which was generally the case for the relatively straight channels in our experiments. Distributions of channel depth are used to calculate a median depth $H_{50}(R)$, which is used in estimates of T_A . We also report channel width statistics as a function of distance from the source.

Next, we characterize “short-timescale” deposition rates in the three active terrestrial environments: channels, wet overbanks, and lobes. Given that overbank deposition should be confined to regions covered by flow, in

the rest of this document we simplify wet overbank to overbank. Here, short-timescale refers to measurements between successive topographic scans, $\delta t = 1$ hr. While deposition rates are dependent on the timescale of measurement (Sadler 1981), all short-timescale rates are calculated over equivalent durations, allowing rates to be compared across environments and between experiments. We construct distributions of short-timescale rates by compiling all rates (including episodes of erosion, stasis, and deposition) for a given environment of deposition, from all run-hours, at a given distance from the source. We then report the 25th, 50th, and 75th percentile of these distributions. We also report bulk statistics of these parameters for the full routing system.

We are also interested in the average profile of deposition in overbank settings as a function of distance from a channel margin, because this allows identification of levee and far-field overbank deposition rates. We identify all overbank cells, measure the distance to the closest channel, and generate a distribution of deposition rates as a function of distance to the closest channel, reporting the 25th, 50th, and 75th percentile of these rates.

Next, we measure long-timescale deposition rates for each experiment as a function of radial distance from the basin source. This is accomplished by differencing our final and initial topographic maps and dividing by the duration of the experiments. We report the 50th percentile of these rates as a function of distance from the basin inlet.

Estimates of avulsion timescales as a function of distance from the basin inlet are made with Eq. 1, measurements of H_{50} , and short-timescale deposition rates from channels and far-field floodplains. Specifically, we find that the median D_{ST} value for overbanks approximates the far-field floodplain deposition rate used in the avulsion timescale equation. We refer to the far-field floodplain as locations past the exponential decrease in deposition rate as a function of distance from a channel that characterizes a levee profile (Pizzuto 1987).

We track the reduction in terrestrial dry fraction of each experimental surface as a function of timespan of observation to estimate T_V . We define f_M as the fraction of the delta-top, measured along radial strike-transects that gets modified by channels, with modification defined as a change in elevation of at least 1 mm, the vertical resolution of our topographic data. Given this, the fraction unmodified by channels (f_{UM}) is equal to $1 - f_M$. We track the change in f_{UM} with timespan of observation over 350-hour time windows, starting every 1 hour of run-time. This time window is sufficient for f_{UM} to decrease to 0.05 for any given starting time in either experiment. For each starting point, we measure the time to f_{UM} reaching 0.05 and then average all measured reduction timescales for a given experiment to get a representative T_V .

We characterize the vertical evolution of our experiments by utilizing the compensation timescale, T_C . For this, we measure the decay of σ_{SS} as a function of timescale of observation (Wang et al. 2011). We use a change-point-detection algorithm that minimizes the squares of the residuals between our data and two power-law trends that intersect at T_C . This allows for the automated detection of T_C and the short and long timescale compensation indexes.

Estimates of T_A , T_V , and T_C then provide the input parameters necessary to estimate T_{ST}^* and T_{ST}^* with Equations 4 and 5.

Characterization of Stratigraphy

We construct a volume of synthetic stratigraphy by stacking topographic maps for each run-hour, which are clipped for episodes of erosion (Strong and Paola 2008). This synthetic stratigraphy can be linked to other known or measured attributes, for example the time of deposition (Fig. 4) or the environment of deposition (Fig. 5B). Each voxel in the stratigraphic volume is assigned an environment of deposition based on the maps that define the surface environments. A comparison of our synthetic stratigraphy to images of the physical stratigraphy indicates that key features like channels and lobes, which are readily apparent in the physical stratigraphy,

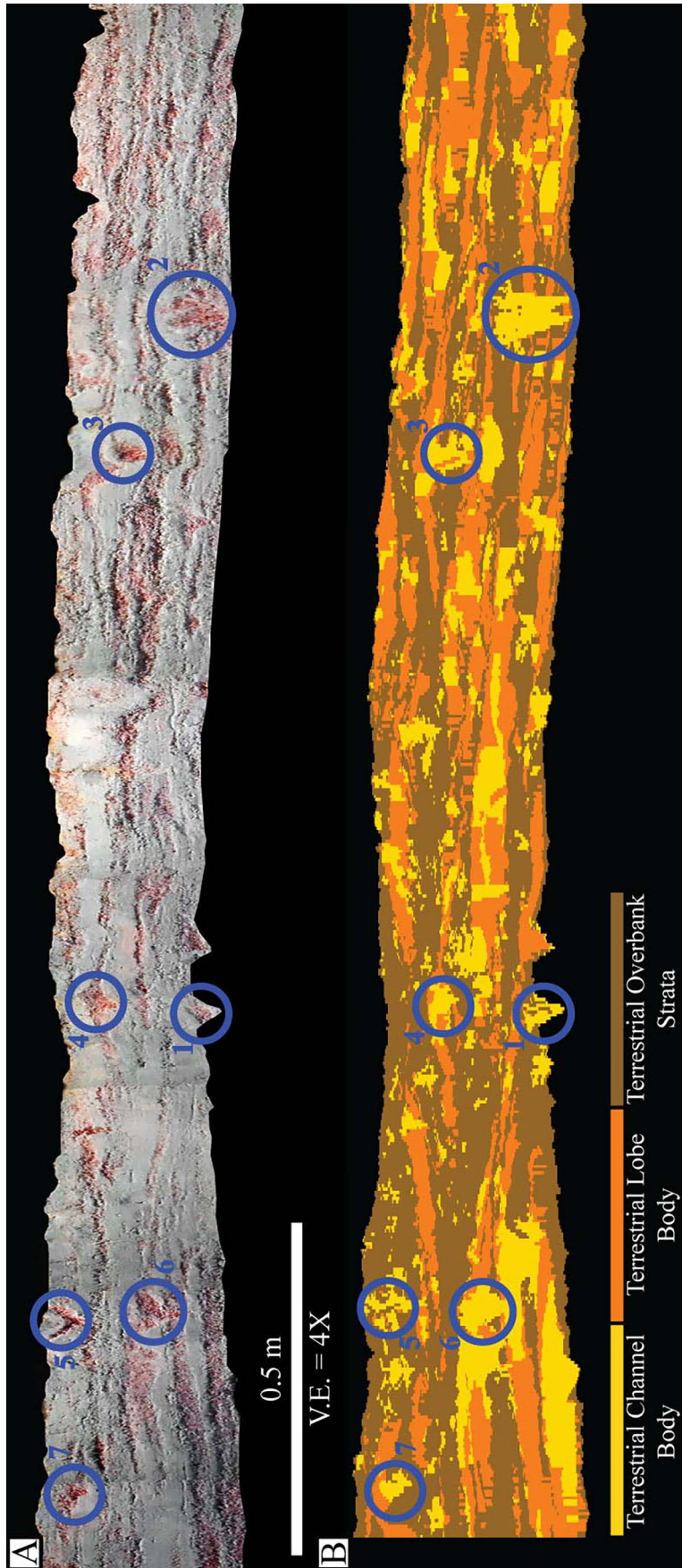


FIG. 5.—Cross-sections of **A**) physical and **B**) synthetic stratigraphy of the low- λ experiment. Cross-section is oriented as if one is looking downstream, with location of cross-section noted in Figure 3D. Synthetic stratigraphy is coded by environment of deposition. Locations of several channel bodies preserved in both the physical and synthetic strata are noted for comparison of the two data types.

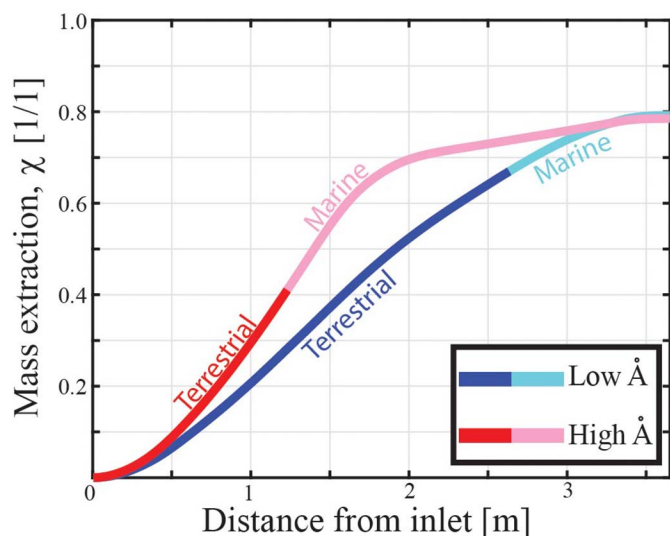


Fig. 6.—Mass-extraction profiles define how distance from source converts to fraction of input sediment extracted to deposition for the two experiments. Dark hues represent dominantly terrestrial settings while lighter hues represent dominantly marine settings.

are correctly categorized in the synthetic stratigraphy (Fig. 5). As such, most of the remaining stratigraphic analysis will utilize the synthetic strata, given the higher spatial resolution at which it was collected, relative to the images of the physical stratigraphy. Synthetic stratigraphy is then used to calculate the fraction of the final deposit associated with each depositional environment.

Constructing a Mass-Extraction Profile

A mass-balance transform for each experiment is constructed using knowledge of the sediment density, known inputs of sediment mass, and measurements of deposit porosities and volumes. We estimate deposit volume as a function of radial distance from the basin inlet using the initial and final topographic scans of each experiment. Next, we fit a polynomial trend to measurements of porosity to estimate porosity at all radial distances from the entrance channel. We then apply Eq. 7 with the known basin geometry and input sediment mass to estimate $\chi(R)$.

RESULTS

Mass-Extraction Profile

Sediment extraction from transport happened over shorter length scales in the high, relative to low, \dot{A} experiment (Fig. 6). A key transition in sediment routing systems is that of the terrestrial to marine environment and associated deposits. As such, we calculate the mean distance from the basin inlet to the shoreline for each experiment and note this transition on the mass-extraction profiles. This transition occurs at χ values of 0.42 and 0.67 for the high- and low- \dot{A} experiments, respectively. In both experiments χ reaches a maximum value of ~ 0.8 at 3.5 m from the basin inlet, a distance that represents the distal wall of the basin and where the basin drain is located. Thus, approximately 20% of the sediment input to the basin was not trapped in the experimental apparatus.

Characterization of Morphodynamics

Morphometrics.—While the inlet water flux and sediment flux for the two experiments was the same, we observe differences in the terrestrial

slope of the deltas, with the slope of the low-accommodation experiment significantly higher than the high-accommodation generation experiment (Fig. 7A). The low \dot{A} slope is approximately constant at 3% for most of the terrestrial reach, before falling close to the mean shoreline location. In contrast, the high \dot{A} experimental slope is approximately 3% just downstream of the entrance channel, but immediately starts to decrease with distance down delta.

We quantify the number of channels observed along strike transects of the experimental surfaces as functions of distance from the basin inlet (Fig. 7B). In each experiment the number of channels initially increases with distance as the inlet channel bifurcated. The median number of channels reaches 4 at a χ value of ~ 0.2 in each experiment. With further distance into the basin the number of channels reduced as autogenic transgressions resulted in rough shorelines that sometimes transgressed to very proximal locations. In addition, some channels end in terrestrial lobes before reaching the shoreline. This trend can also be linked to the observation that very long terrestrial channels, with river mouths at distal basin locations, are generally linked to a condition where a single and very efficient channel for sediment transport forms, in contrast to more bifurcated networks. In mass-balance space the two experiments share similar channel numbers along strike transects as a function of χ . This finding suggests that in mass-balance space, differences in T_V should solely be linked to differences in the mobility of individual channels.

Statistics that characterize channel depths also share similar trends in mass-balance space. In each experiment H_{50} peaks just downstream of the basin inlet (Fig. 7C). Channels then rapidly lose relief before maintaining approximately constant relief with further distance into the basin. Bulk statistics of channel depths over the full routing systems show tremendous overlap between experiments with similar mean values. Channel widths, however, were significantly different in the two experiments, both in dimensional distance from the basin inlet and in mass-balance space (Fig. 7D). Bulk statistics for the full routing systems show that channels were approximately 30% wider in the high-accommodation experiment than in the low-accommodation experiment. Taken together, differences in channel widths and delta-top slope between experiments highlights that these parameters are not only controlled by the ratio of $Q_s:Q_w$.

Depositional Statistics

In systems with constant boundary conditions, deposition rates are a function of timespan of measurement for timescales less than T_C (Schumer and Jerolmack 2009; Straub et al. 2020). Therefore, we present measurements of both short- and long-timescale deposition rates to capture both shorter-term morphodynamics and longer-term deposition. In each experiment, mean overbank D_{ST} gradually decreases with down-basin distance, asymptoting at a value of ~ 0.1 mm/hr (Fig. 8A). The distributions of overbank deposition rates for the entire transport system show tremendous overlap between experiments; part of this overlap is likely due to the measurement precision of our topography scanner. However, the quantity of overbank measurements per experiment (in excess of 10^6) allows us to identify a 50% greater overbank D_{ST} in the high-accommodation experiment than in the low-accommodation experiment, with a standard error of the mean below one micron. In contrast, in-channel D_{ST} is markedly greater in the high \dot{A} , relative to low \dot{A} , experiment (Fig. 8B). This holds whether viewed in a distance from source, mass-balance, or bulk transport system perspective. In both experiments in-channel D_{ST} gradually increases with distance into the basin before rapidly increasing near the shoreline. Short-timescale lobe deposition rates are relatively independent of distance into the basin and show a slight dependence on \dot{A} . Averaged over the full transport system, lobe D_{ST} is 29% greater in the high- vs. low- \dot{A} experiment (Fig. 8C). We also measured the dependence of short-timespan overbank deposition rates on distance from a channel (Fig. 9). Close-to-channels overbank deposition rates are slightly greater in the high- \dot{A} , relative to low- \dot{A} experiment. Similar to field systems, we note an

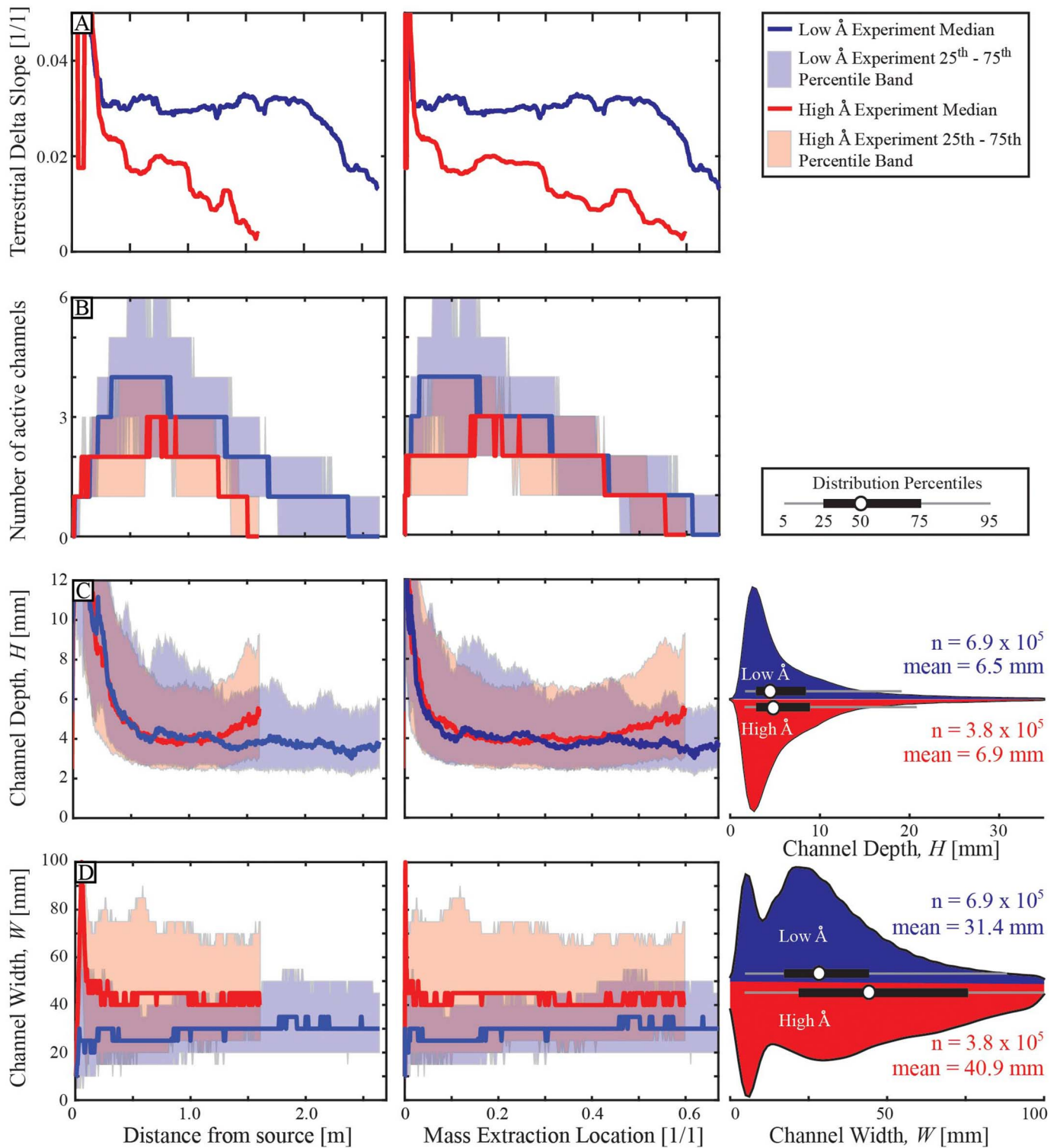


FIG. 7.—Data defining key morphological parameters as a function of distance from source (left panels), mass-extraction location (center panels), and bulk statistics, presented as violin plots, for the full routing system (right panels) of each experiment. **A)** Data defining the down-delta terrestrial slope. **B)** Data defining number of active channels on a given surface. **C)** Data defining depth of active channels on a given surface. **D)** Data defining width of active channels on a given surface. Lines in left and center panels represent median values, while semitransparent shaded regions spanning the 25th–75th percentiles.

exponential decrease in deposition rates as a function of distance from the closest channel until rates stabilize at their far-field values (Pizzuto 1987). In both experiments this value is ~ 0.1 mm/hr, suggesting that far-field over-bank deposition rates are not a function of \bar{A} .

Long-term deposition rates, measured between the start and the end of each experiment, are consistently greater in the high- \bar{A} , relative to low- \bar{A} experiment (Fig. 8D). While measured rates approximately equal imposed base-level rise rates in the high- \bar{A} experiment, we note that

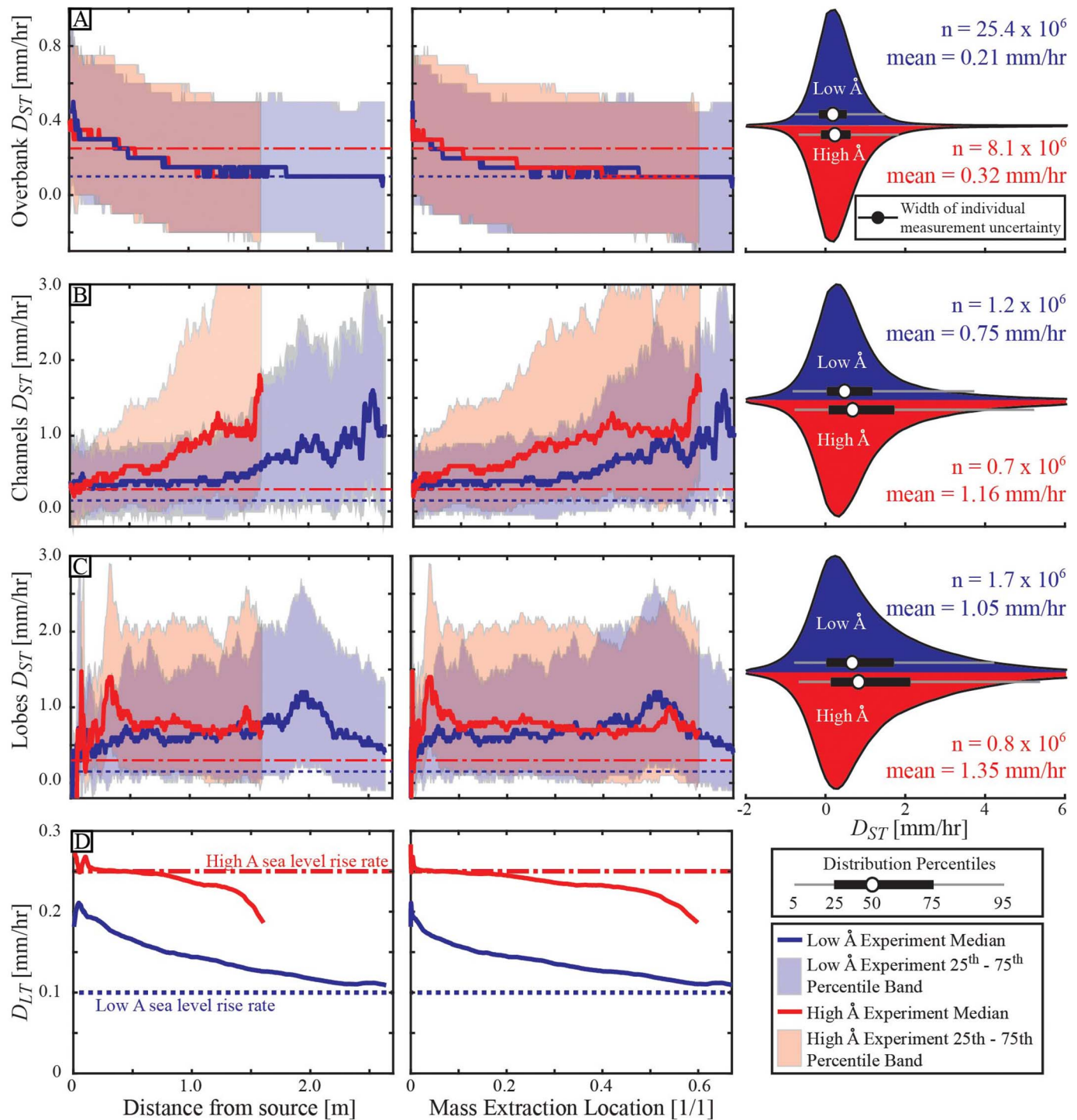


FIG. 8.—Data defining short ($\delta t = 1$ hr) and long ($\delta t = 560$ hr) timescale deposition rates as a function of distance from source (left panels), mass-extraction location (center panels), and bulk statistics, presented as violin plots, for the full routing system (right panels) of each experiment. Short-timescale deposition rates presented for A) overbank, B) terrestrial channel, and C) terrestrial lobe depositional environments. Lines in left and center panels represent median values, while semitransparent shaded regions spanning the 25th–75th percentiles. D) Data defining long-term deposition rates of bulk deposit as a function of position in basin for each experiment. Dashed lines illustrate imposed long-term sea-level rise rate in each experiment.

D_{LT} outpaces base-level rise rates in the low- \dot{A} experiment. Further, D_{LT} decreases with distance into the basin in this experiment. Combined, these observations suggest that the delta slope and area were not completely in dynamic equilibrium with forcing conditions at the start of the low- \dot{A} experiment aggradation stage. As a result, the experimental

surface slope increased from 0.022 m/m to 0.033 m/m from the start to end of this experiment.

In addition to rates of deposition, we also measure the propensity of deposition to occur in topographic lows. Compensation statistics over autogenic basin-filling timescales, which measure this propensity, are similar in

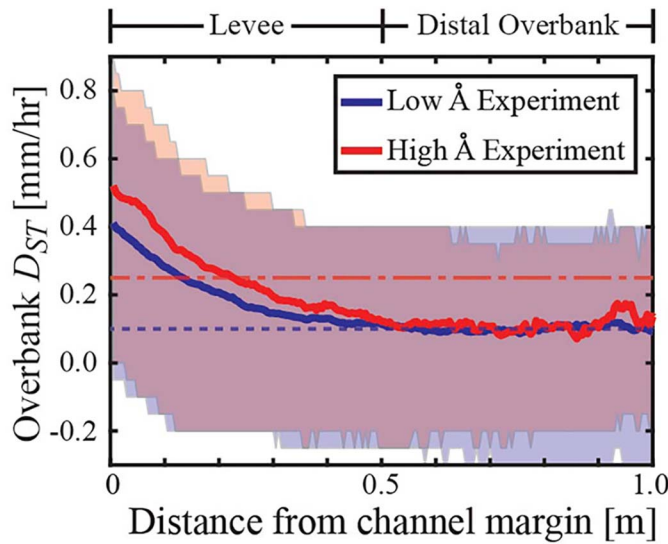


FIG. 9.—Data defining short-term deposition rates as a function of distance from the closest active channel for each experiment. Lines represent median values, while semitransparent shaded regions span the 25th–75th percentiles. Dashed lines illustrate imposed long-term sea-level rise rate in each experiment.

the two experiments. Specifically, the short-timescale compensation index, κ_{ST} , does not vary strongly with distance into the basin for the two experiments, carrying a value of ~ 0.4 (Fig. 10). This suggests that over autogenic timescales there is a slight preference for persistence in depositional trends, in contrast to compensational deposition in topographic lows. This depositional persistence roughens topography until large-scale compensational relocation of transport systems occurs at a timescale equivalent to T_C .

Autogenic Timescales

Next, we use our morphodynamic measurements and maps of depositional environments to quantify key autogenic timescales. The shortest autogenic timescale explored is the avulsion timescale, T_A . We emphasize here that T_A is an estimated setup timescale for avulsions, and not a timescale between measured avulsion events. However, theory suggests that T_A should scale with the time between observed avulsion events (Jerolmack and Mohrig 2007; Hajek and Wolinsky 2012). Using Eq. 1, measurements of H_{50} , and short-timescale deposition rates, we estimate a decrease in T_A with distance into each experiment (Fig. 11A). This trend is driven by

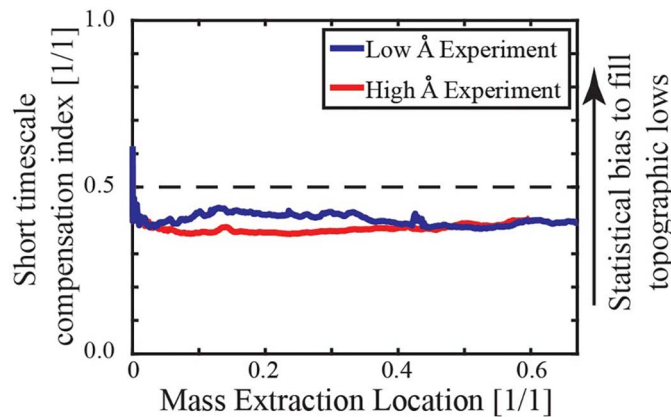


FIG. 10.—Measurements of short-timescale compensation indexes as a function of mass-balance location in each experiment.

measured decreases in channel depths (Fig. 7B) and increases in channel deposition rates (Fig. 8B) with distance into the basin. While the T_A vs. χ trend is similar in shape for the two experiments, T_A is consistently longer in the low- \bar{A} , relative to high- \bar{A} , experiment, primarily due to the difference in channel D_{ST} between experiments.

While T_A quantifies a setup time for an individual channel avulsion, T_C quantifies the time necessary for the products of autogenic channel movements, including avulsions, to average out in the structure of the basin fill (Wang et al. 2011). In the high- \bar{A} experiment, we observe relatively constant T_C values until reaching locations near the mean shoreline, where T_C starts to rise (Fig. 11B). This is likely due to a reduction in long-term deposition rates past the mean shoreline and larger roughness scales associated with the delta front (Trampush et al. 2017). In contrast, T_C initially increases with χ in the low- \bar{A} experiment, until stabilizing at a nearly constant value with further increases in T_C (Fig. 11B). Here, the initial increase is likely due to the reduction in long-term deposition rates with χ that occurred in proximal regions of this experiment. Over the region where T_C was stable with χ in the two experiments, we note approximately two-fold greater T_C values in the low- \bar{A} , relative to high- \bar{A} experiment (Fig. 11B).

The final autogenic timescale, T_V , quantifies the amount of time necessary for a significant fraction of the terrestrial delta-top to be modified by channelized flow. Between χ values of 0 to 0.4, we observe approximately spatially constant visitation timescales that differ between experiments by approximately a factor of 2, with this autogenic timescale again being greater in the low- \bar{A} , relative to high- \bar{A} , experiment (Fig. 11C). In both experiments T_V increases with further distance into the basin.

Basin Mobility Metrics

The measured autogenic timescales suggest that accommodation production rates scale with rates of autogenic processes (i.e., higher \bar{A} , shorter autogenic timescales). A key question, however, is whether some autogenic rates are more sensitive to accommodation production than others. To explore this, we look at ratios of autogenic timescales. For example, if T_C/T_A (T_{ST}^*) varies as a function of accommodation production, it would indicate that the number of avulsions during a compensation timescale should vary, which should have implications for stratigraphic architecture. The ratio of T_C to T_V (T_{LT}^*) should also carry stratigraphic-architecture implications, because T_C describes the vertical mobility of a transport system while T_V describes a system’s lateral mobility. Starting with T_{ST}^* , we observe a systematic increase in this metric with distance into the basin, suggesting that channels are more prone to avulse at distal basin locations (Fig. 12A). However, in mass-balance space T_{ST}^* is approximately equal in the two experiments at equivalent χ locations. In a similar fashion, values of T_{LT}^* are approximately equal at equivalent χ values in the two experiments (Fig. 12B). This suggests that changes in the vertical mobility of each system (i.e., aggradation), driven by changes in accommodation production, induce proportional changes in lateral mobility.

Characterization of Strata

A central goal of this study is to explore the capacity of mass-balance transformations to aid prediction of gradients in facies linked to critical depositional environments. As such, we first quantify how much overbank strata was preserved in the two experiments, in addition to quantifying the fraction of each deposit linked to other depositional environments. This is achieved with the synthetic stratigraphy coded such that each voxel within the volume is linked to an environment of deposition (Fig. 13). We confirm that both experiments had significant preservation of overbank strata, at 29% and 18% in the low- \bar{A} and high- \bar{A} experiments, respectively. If we focus just on the terrestrial deposits, the fraction of strata linked to overbank deposition increases to 43% and 36%, respectively, for the low- \bar{A} and high- \bar{A} experiments (Fig. 13). A second observation is the large fraction of

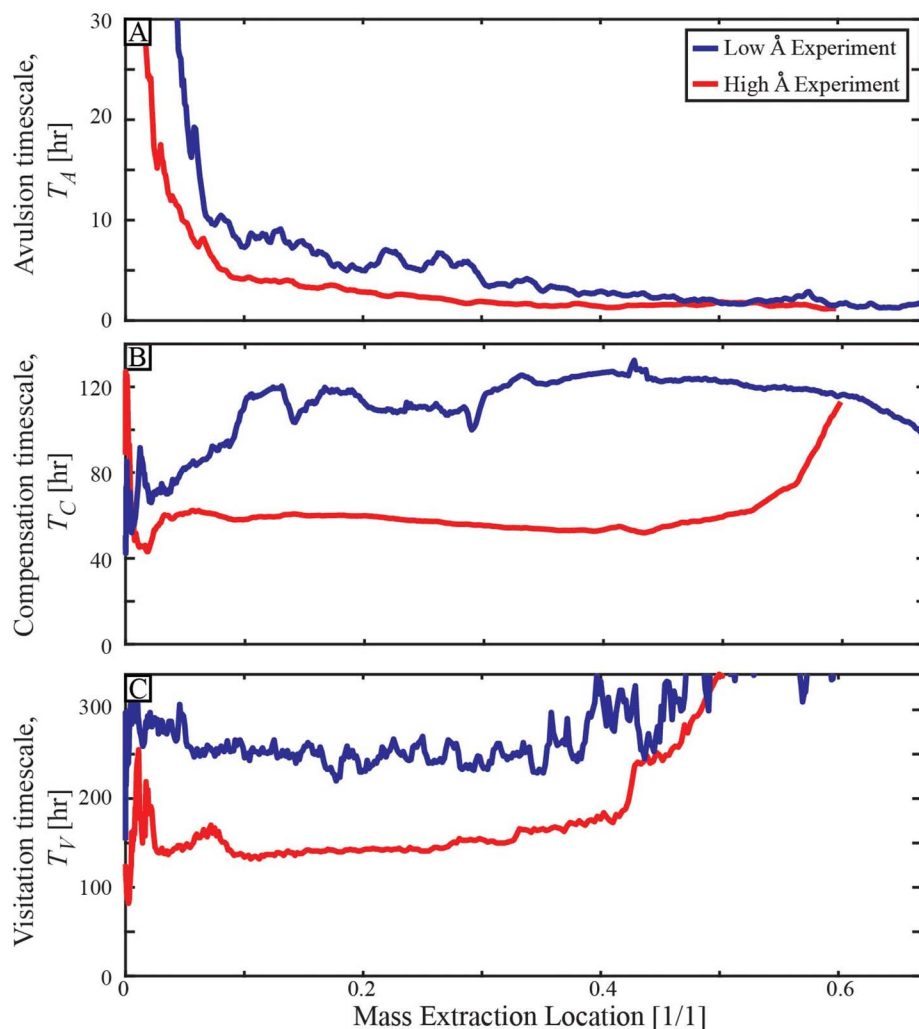


FIG. 11.—Estimates and measurements of autogenic timescales as a function of mass-balance location in each experiment. **A)** Estimates of avulsion-setup timescales made with measured median channel depths and short-timescale deposition rates. **B)** Measurements of compensation timescales made from measurements of the decay of σ_{SS} with timespan of observation. **C)** Measured channel-visitation timescales for experimental surfaces.

sediment in each experiment deposited in the marine, particularly in the high- \bar{A} experiment where 50% was deposited in the marine. A significant export of sediment to the marine is in line with many large river deltas, where terrestrial sediment retention rates are often less than 50% (Goodbred and Kuehl 1998; Kim et al. 2009). We note that in both experiments a fraction of the deposit ($< 10\%$) is coded dry land. This represents errors in our coding scheme, likely due to environments of deposition changing over timescales below our measurement frequency. For example, this could represent a brief episode of overbanking flow between sequential topographic maps, or a brief episode of terrestrial lobe deposition associated with a crevasse splay.

Next, we utilize our synthetic stratigraphy to quantify gradients in deposit fraction linked to each depositional environment. In both experiments we find that the fraction of strata coded as channel bodies decreases with distance into the basin (Fig. 14A). The fraction of channel strata drops to 0 at ~ 2 m from the basin entrance in the high-accommodation-production experiment. Loss of channel deposits does not occur until a distance greater than 3.2 m from the source in the low-accommodation-production experiment. The distance from the source at which channel deposition goes to zero represents the most distal location of shorelines in each experiment. However, when channel deposit fraction is presented in mass-balance space the data from the two experiments approximately collapse onto a single trend (Fig. 14A).

The fraction of lobe deposits preserved in each experiment, as a function of distance from the source, follows parabolic curves. In mass-balance

space the lobe fraction is nearly identical in the two experiments up to a χ value of 0.4 and then decays with further distance into the high- \bar{A} experiment, while this decay does not begin until a χ value of ~ 0.6 in the low- \bar{A} experiment (Fig. 14B).

Terrestrial overbank deposit fraction decreases with distance into each experiment (Fig. 14C), which conforms with our observation of reduced short-timescale overbank deposition rates with distance into the basin (Fig. 8A). Loss of overbank deposits occurs at a similar distance into the basin where channel and lobe deposits are lost. In mass-balance space the decay rate of overbank deposits is similar in the two experiments, but the low- \bar{A} experiment consistently has greater overbank deposit fractions by approximately 10%.

The last depositional environment is the marine. We observe marine deposition occurring at χ values as low as 0.2 in the high- \bar{A} experiment. Marine deposition is not preserved until a χ value of 0.6 in the low- \bar{A} experiment. While preservation of marine strata begins at different χ values in the two experiments, preservation of any terrestrial strata ceases at a χ value of ~ 0.7 in both experiments (Fig. 14D).

We explore stratigraphic architecture in the two experiments in sections that are approximately strike oriented and represent the physical stratigraphy paired with panels of synthetic stratigraphy colored by environment of deposition (Fig. 15). While we define our mass-balance framework with radial distance from the entrance to the basin, here we present panels that are perpendicular to the long wall of our basin, because this is how our images of the physical stratigraphy were collected. We present locations that were dominated by terrestrial

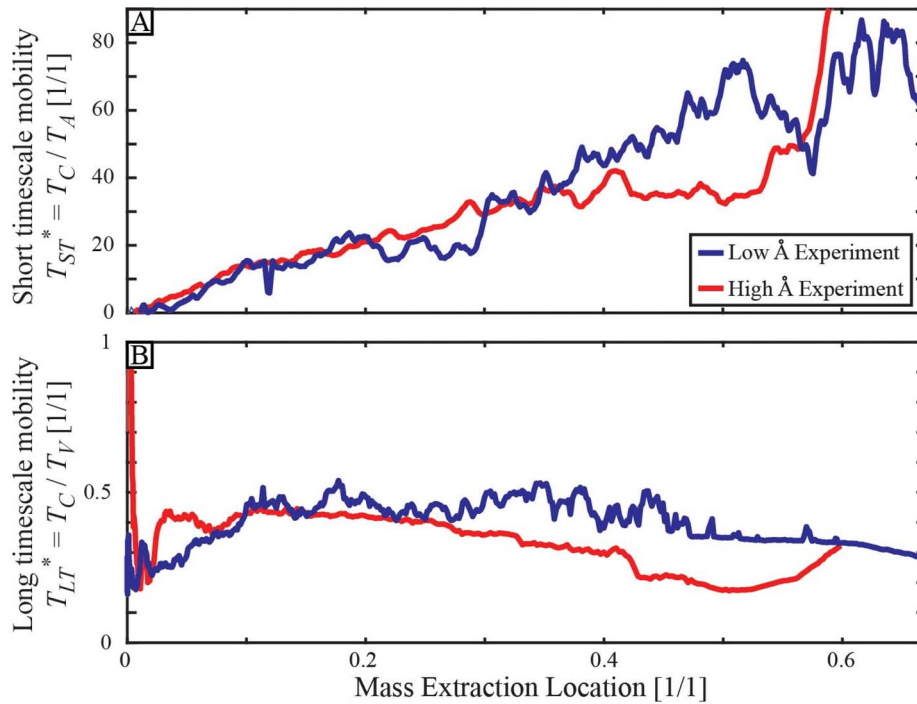


FIG. 12.—Mobility metrics generated with ratios of autogenic timescales as a function of mass-balance location in each experiment. **A)** Ratio of compensation to avulsion timescale, T_{ST}^* . **B)** Ratio of compensation to visitation timescale, T_{LT}^* . Similar basin-mobility metrics at a given mass-balance location suggests that strata should have similar architecture.

deposition, corresponding to χ values of ~ 0.2 and 0.3 (Fig. 14). While many similarities exist for stratigraphic panels from the two experiments, we note some differences. First, preserved channel bodies appear to be wider in the high- \dot{A} experiment relative to low- \dot{A} experiment (Fig. 15). This might be due to the wider channels measured on the surface in the high- \dot{A} experiment, or due to greater lateral migration rates in this experiment. The latter would suggest greater prevalence of channel-belt deposits, in comparison to channel-body deposits in the high- \dot{A} experiment. Second, channel bodies in the low- \dot{A} experiment are generally thicker, suggesting greater in-channel aggradation between avulsion events (Fig. 15).

DISCUSSION

Coupling of Autogenic Timescales

As a recap, we focus on three autogenic timescales: 1) the avulsion timescale, T_A , defined as the time to superelevate a channel by one channel depth, 2) the visitation timescale, T_V , defined as the time necessary for 95% of the deltaic surface to be visited by channels that do geomorphic work, and 3) the compensation timescale, T_C , defined as the time necessary for depositional patterns to mimic patterns of accommodation production. While accommodation production rates influence autogenic process

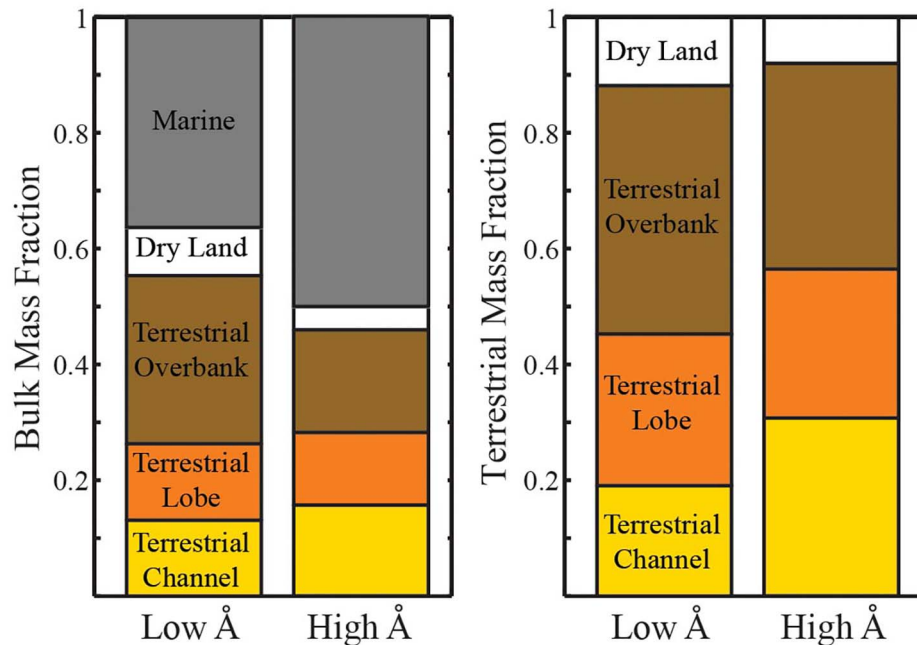


FIG. 13.—Data defining fraction of deposit associated with each depositional environment for the two experiments. **A)** Fraction of bulk deposit associated with each depositional environment. **B)** Fraction of terrestrial strata linked to each terrestrial depositional environment.

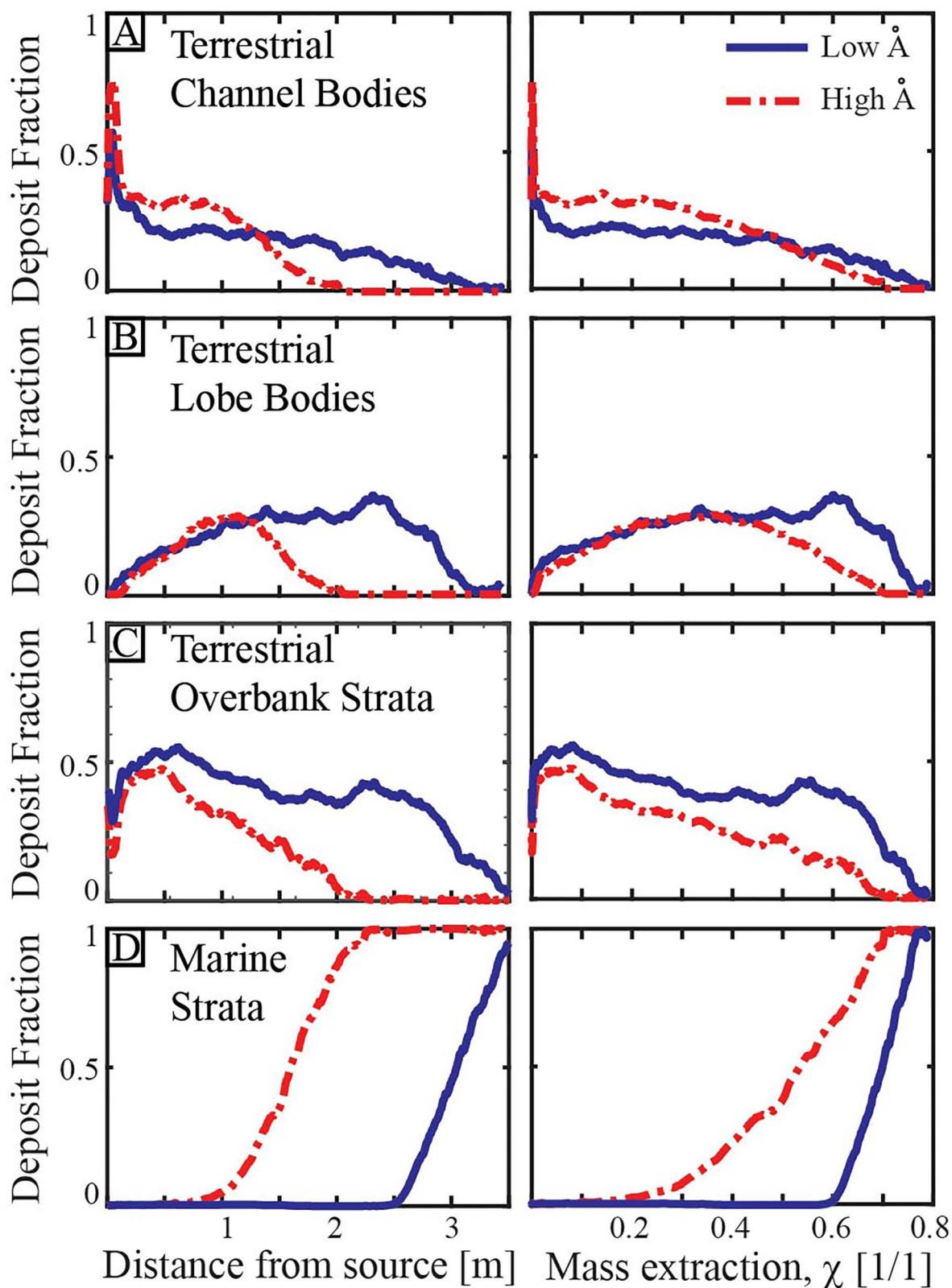


FIG. 14.—Data defining fractions of bulk deposits linked to each depositional environment as a function of dimensional distance from source (left panels) and mass-extraction location (right panels) for each experiment. Environments of deposition include A) terrestrial channels, B) terrestrial lobes, C) terrestrial overbank, and D) marine.

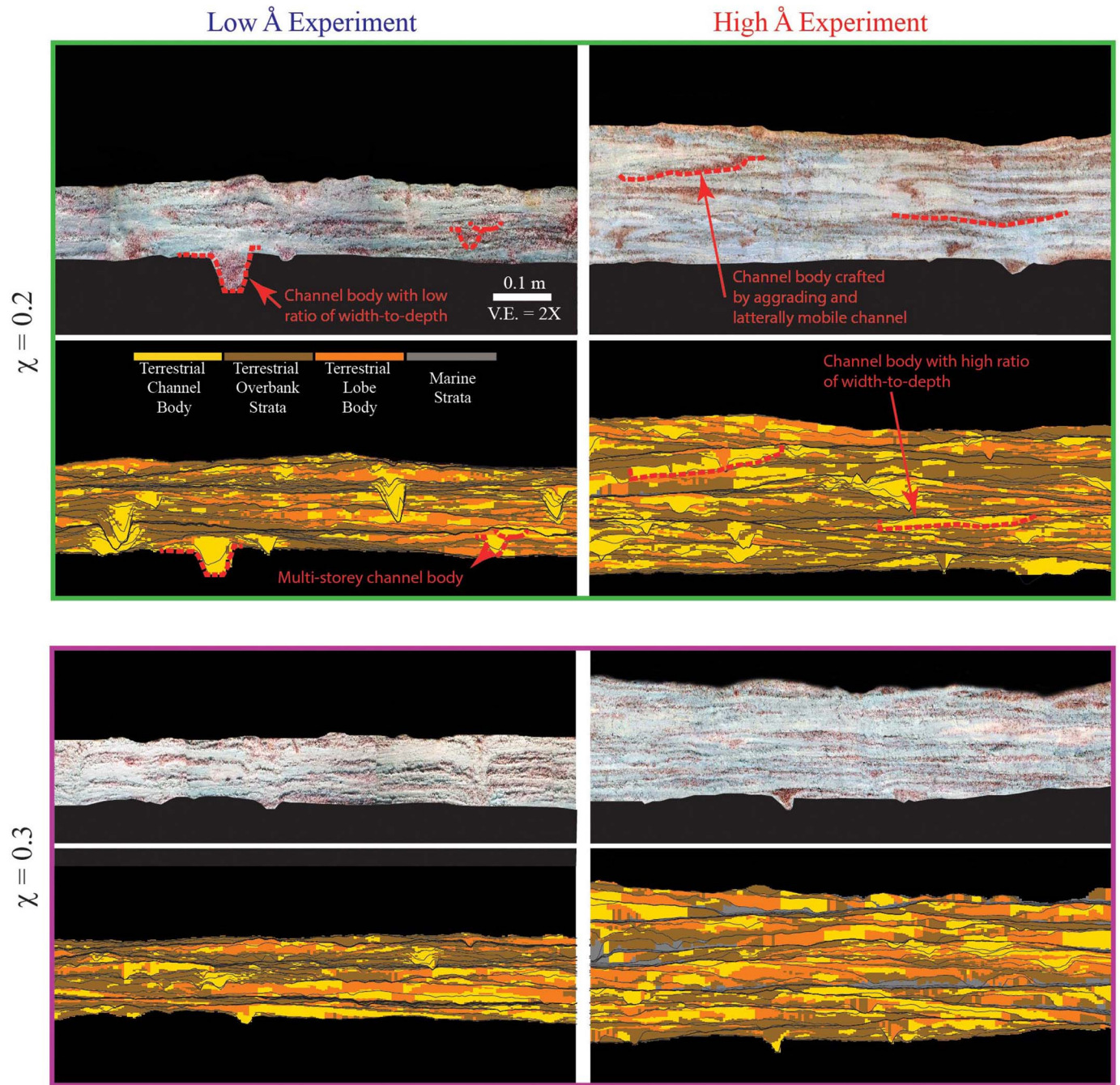


FIG. 15.—Cross-sections of physical and synthetic stratigraphy produced in the two experiments. All panels are oriented perpendicular to the long wall of the experimental basin, making them approximately strike-oriented sections. Sections are presented with sediment transport into the panels and come from the middle third of the full basin cross-section. Given that our mass-balance framework is defined as a function of radial distance from the source, mass-balance position of each cross-section is approximate. Solid black lines are timelines of the synthetic strata, generated by stacking topographic scans and clipping for episodes of erosion. Timelines are presented for every 10th hour of each experiment.

timescales, a key finding of this study is that they do so in a manner that preserves mobility metrics important for stratigraphic architecture (Fig. 12). We find, perhaps unsurprisingly, that changes in accommodation production influence compensation timescales in our experiments (Fig. 11B). Differences in T_C between experiments were primarily due to differences in the long-timescale deposition rates, as channel depths were similar.

Similar to our experiments, other experimental studies have documented increases in channel mobility, specifically avulsion rates, with an increase in

sedimentation rates (Bryant et al. 1995; Hickson et al. 2005; Martin et al. 2009; Chadwick et al. 2020). A known method to increase delta-top sedimentation is to increase local accommodation production rates, either through enhanced subsidence or sea-level rise (Muto and Steel 1997). The response of the routing system to this increase in accommodation is felt first and perhaps strongest in the channels, increasing channel deposition rates. This decreases the timescale necessary to achieve the avulsion setup condition (Eq. 1).

While avulsion, compensation, and visitation timescales scale inversely with accommodation production (Fig. 11), they proportionately changed by the same amount when viewed in mass-balance space (Fig. 12). Thus, in mass-balance space the propensity for channels to avulse during the basin-wide aggradation of a compensation length scale is equivalent. A similar self-organization is observed in the proportional changes to T_C and T_V . The compensation scale characterizes the average amount of deposition necessary for autogenic process, largely associated with lateral migration of the transport system, to average out. In contrast, the visitation timescale is a description of the lateral mobility of a system, averaged over a time-scale long enough for channels to visit a significant fraction of a basin. While both T_C and T_V characterize the filling of basins, they are not identical. Systems with high lateral mobility, relative to aggradation rates, will visit and rework topography multiple times during the aggradation of one compensation scale, resulting in more reworking of the active layer and the potential for multi-story channel bodies (Straub and Esposito 2013). Similar values for T_{LT}^* observed in our two experiments (Fig. 12B) likely explain the similar propensity for deposition to occur in topographic lows, as quantified by κ_{ST} (Fig. 10). Further, the similar trends in our long-timescale mobility metric, T_{LT}^* , as a function of χ suggest that the lateral mobility of transport systems is directly and proportionately linked to the self-organization of topography and deposition rates, which are set by accommodation production. This self-organization, coupled with comparable gradients in our short- and long-timescale mobility metrics, suggests similar densities of strata tied to specific depositional environments in the two experiments. For example, the observed trend in T_{LT}^* with χ suggests similar channel-body density as a function of χ in the two experiments, which is what our stratigraphic analysis reveals (Fig. 14A). These observations, which come from experiments that preserve significant overbank strata, support earlier mass-balance studies focused on bedload-dominated systems that highlight the importance of mass-extraction to preserved depositional environmental gradients in fluvial strata (Strong et al. 2005). Our addition is the suggestion that self-similar facies gradients (Fig. 14) are a result of the self-organized manner that key autogenic surface processes respond to the production of accommodation (Fig. 12).

The work of Strong et al. (2005) and Paola and Martin (2012) suggests that sedimentary basins sharing similar forcings, with the exception of accommodation production, should share similar depositional-environment gradients in a mass-balance space. They also suggest that some critical transitions in preserved depositional environments, for example transitions from strata dominated by channel bodies to lobe deposits, might occur at somewhat universal χ values ($\chi = 0.8$ for the channel-to-lobe transition). Here, we briefly summarize down-basin changes in the fraction of different preserved depositional environments in our experimental strata and differences in stratigraphic architecture. First, in mass-balance space we note similar trends for the fraction of strata composed of channel bodies (Fig. 14A), which we suggest is linked to similar basin mobility metrics and compensation statistics in our experiments (Fig. 12). We note that the autogenic timescales explored are rather channel-centric, and so the link between measured timescales and stratigraphic products should be strongest for this depositional environment. While channel deposit fractions were similar in the two experiments, the high- \dot{A} experiment had channel story complexes that indicate a large amount of lateral migration paired with slow aggradation (Figs. 15, 16). In contrast, the low- \dot{A} experiment had relatively narrow and deep channel story complexes. Strata of both experiments preserves records of channel reoccupation, through multistory channel bodies (Figs. 15, 16). In locations that were dominantly terrestrial ($\chi < 0.4$) both experiments share similar values for the fraction of strata composed of terminal lobes (Fig. 14B), but at higher χ values the experiments diverge in lobe-strata abundance. Unlike prior mass-balance studies (Paola and Martin 2012), we do not see a sharp transition between channel-body-dominated vs. lobe-dominated strata at a $\chi = 0.8$, but rather strong overlap in the spatial abundance of these stratigraphic products (Figs. 14–16). While both experimental deposits have a reduction in terrestrial overbank strata with χ , the low-

\dot{A} experiment shows consistently higher overbank deposit fractions (Fig. 14C). Finally, we note that one critical depositional boundary, terrestrial to marine strata, is located at markedly different χ values in the two experiments (0.42 vs. 0.67 in the high- \dot{A} vs. low- \dot{A} experiments, respectively) (Fig. 6). Thus, at first take it appears that the mass-balance framework's predictive power is strongest for the channelized or other bedload-dominated strata and reduces as one moves towards facies dominated by suspension-fallout deposition. We stress that applying or testing these findings to field strata would require generation of sediment budgets, as done in Hampson et al. (2014) and Sincavage et al. (2019).

We explore one process that might influence facies transitions and the abundance of preserved depositional environments in the two experiments: advective settling of fine particles overbanking channel banks. A key aspect of our experimental forcing is the use of a wide distribution of particle sizes, with abundant particles in the silt and finer size range. Visual observations of the experiments confirmed that only fine particles were transported in suspension and leaked to the floodplains. We estimate an advection settling length for particles that overbank channels in our experiments and compare this to the distance from the basin entrance to mean shoreline location. Ganti et al. (2014) defined an advection settling length, l_a , as

$$l_a = \frac{uh_S}{w_S} \quad (8)$$

where u is a characteristic flow velocity, h_S is a settling height, and w_S is a particle fall velocity. This length scale is most accurate for defining particle transport distances in relatively quiescent flows, such as those found in floodplains (Ganti et al. 2014). While a distribution of l_a would characterize our experiments, we make a singular and rough estimate with the following assumptions. First, we assume that flow in channels is approximately Froude critical, supported by earlier observations of similar experimental systems (Hoyal and Sheets 2009). Assuming a characteristic channel depth of 10 mm, the assumption of Froude criticality allows us to estimate a characteristic flow velocity. Our choice of a 10 mm channel depth, which is larger than H_{50} , accounts for the fact that deeper channels contribute a disproportionate long-term mean sediment flux given the nonlinear relationship between channel size and sediment flux rates (Nittrouer et al. 2011). We use this velocity to describe overbanking flow, and given the largely constructional nature of channels in the experiments, we assume a settling height also of 10 mm. Finally, we use the Ferguson and Church (2004) method to calculate a settling velocity for the D_{50} of the experimental sediment mixture (67 μm) equal to 3.3 mm/s. This will likely overestimate fall velocity of the overbanking particles, which were likely finer than the D_{50} of the input sediment to the basin. These assumptions result in an advection settling length of ~ 0.9 m. A similar set of calculations for the D_5 , D_{25} , D_{75} , and D_{95} produce advection lengths of approximately 5 km, 9 m, 0.2 m, and 40 mm, respectively. While the assumptions above carry significant uncertainty, it highlights that in the high- \dot{A} experiment a significant fraction of sediment leaked to the overbank could advect to the shoreline and into the marine before deposition, as the mean radius of this delta was only 1.2 m. In contrast, the mean radius of the low- \dot{A} experiment was 2.7 m, and so a higher fraction of overbanking sediment should get trapped in the terrestrial in this experiment. We suggest that this helps explain the difference in terrestrial trapping efficiencies and the fraction of strata linked to overbank sedimentation in the two experiments.

We estimate field-scale advection lengths to explore the propensity of overbanking particles to advect past shorelines. Again, a range of advection lengths would characterize any database of deltas, but for simplicity we use a settling velocity of flocculated overbanking clays, recently reported by Lamb et al. (2020) equal to 0.35 mm/s, a typical fluvial flow velocity of 1 m/s, and a settling height for overbanking flow of 5 m, based on natural-levee heights for larger river systems (Nittrouer et al. 2012). Combined, this yields an advection length of ~ 15 km, a distance that is

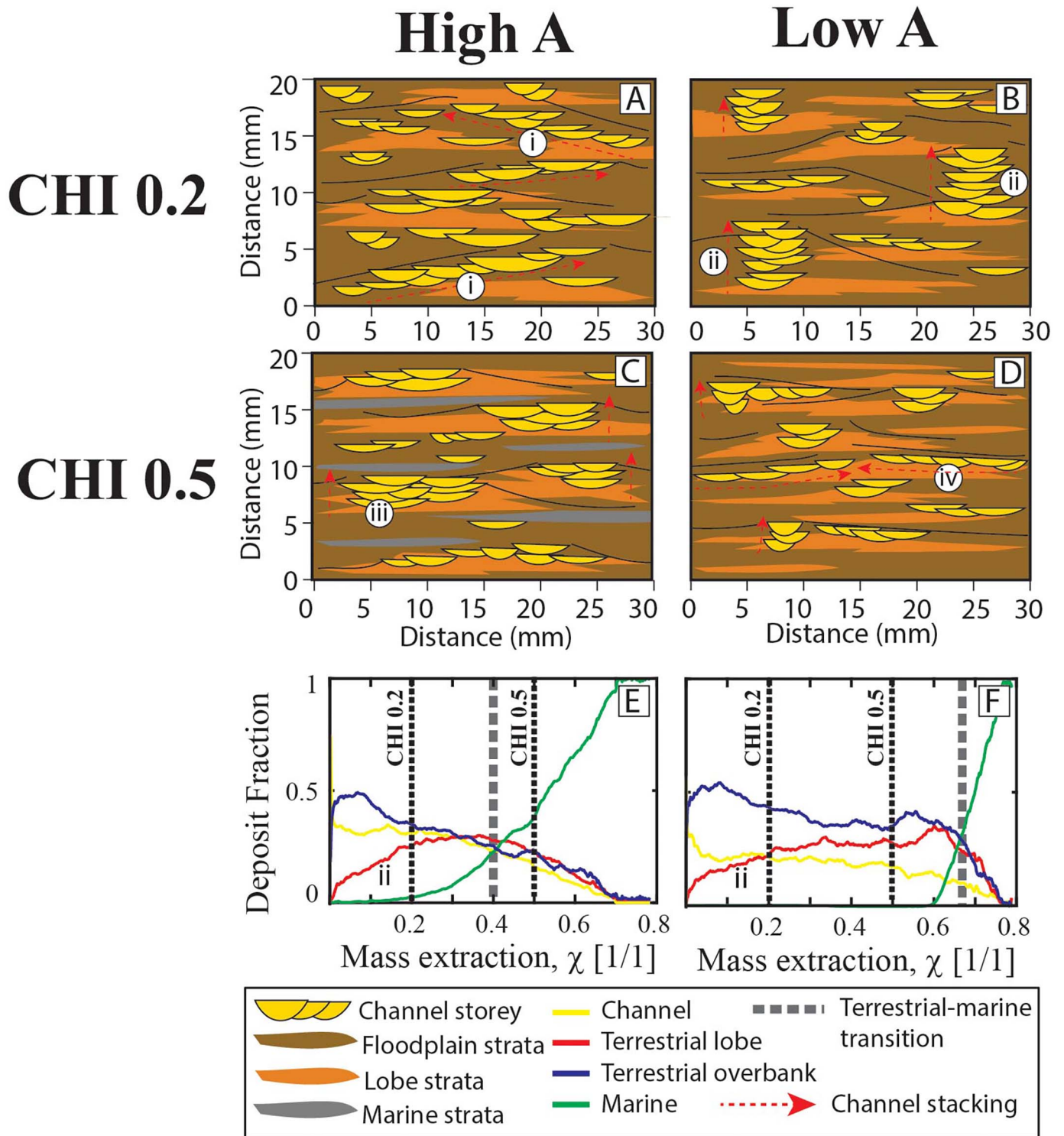


FIG. 16.—A, C) Schematic cross sections of the sedimentary architecture at CHI = 0.2 and CHI = 0.5 for the high-accommodation experiment and B, D) the low-accommodation experiment. Numerals refer to: i) multi-story, multilateral offset stacked channel architecture with high trajectory, ii) multi-story, vertically stacked channel architecture (thickness \gg channel depth), iii) multi-story nested and nested offset stacked channel architecture, iv) multi-story, multilateral offset stacked channel architecture with low trajectory, vi) multi-story, vertically stacked channel architecture (thickness \geq channel depth). E, F) Fraction of deposit composed of either channel, overbank, lobe, and marine strata for the high-accommodation experiment (left) and the low-accommodation experiment (right).

significantly smaller than the radius of many large river systems (Jerolmack 2009). This suggests that while sediment overbanking levees near shorelines could be lost to the marine, over the fluvial and much of the deltaic transport segment overbanking particles will get trapped in terrestrial overbank settings. The advection length will vary with grain size in channelized transport, with coarser systems experiencing less leakage of overbank sediment to the marine (and likely less sediment leakage out of channels to begin with). It will also depend on the settling height of overbanking sediment, with smaller systems linked to lower settling heights. Combined, grain-size and system-size influence on advection length scales for overbanking particles likely also carry a signature of tectonic setting. For example, we hypothesize more overbanking sediment in large, fine grained passive margin systems relative to smaller and steeper routing systems along active tectonic margins and likely more leakage to the marine. We suggest that in regions where advection length scales are less than the distance to a shoreline, a mass-balance framework should carry predictive power for all facies gradients in strata. This analysis also emphasizes that application of a mass-balance framework to predict stratigraphic architecture can be enhanced by considering the total length of a transport segment, in addition to average accumulation rates, inasmuch as longer systems will almost always trap more sediment, all else being equal.

Returning to the Role of Accommodation Production on Stratigraphic Architecture

Our results, which come from experiments in which only accommodation production rate was varied, and which included overbank strata resulting from suspension fallout, share similar fractions of deposits produced in key depositional environments in a mass-balance space. As such, our results suggest that channel-body density is independent of accommodation production rate in a mass-balance space, supporting earlier mass-balance studies (Paola and Martin 2012; Strong et al. 2005). This finding also helps explain the results of the meta-study performed by Colombera et al. (2015), which found that channel-body density, geometry, and stacking pattern are not reliable diagnostic indicators of accommodation production rates. Similar to the theoretical framework provided by Paola and Martin (2012), we suggest that mass-balance frameworks help collapse stratigraphic observations because they allow comparison of locations with similar $Q_s:Q_w$ ratios. This stratigraphic finding follows on decades of work that highlights the importance of $Q_s:Q_w$ on surface morphology and dynamics (Parker et al. 1998; Whipple et al. 1998; Powell et al. 2012; Wickert et al. 2013). While channel-body density was similar in the two experiments, we do note differences in both the width of channels and preserved channel bodies in the strata (Figs. 15, 16). Differences in the surface slopes were also observed between experiments. This highlights that while $Q_s:Q_w$ critically influences channel width and slopes, other secondary factors also come into play and should be considered when inverting strata for paleoenvironmental conditions.

The experimental sediment mixture used in this study allows us to explore the role of accommodation production on overbank sedimentation and stratigraphic architecture. We see tremendous overlap in the overbank depositional statistics in the two experiments (Figs. 8A, 9). However, the vast number of D_{ST} measurements in this study allow us to identify the following differences. First, greater deposition rates near levee crest were measured in the high- \bar{A} vs. low- \bar{A} experiment (Fig. 9). Second, a 50% greater mean overbank deposition rate was measured in high- \bar{A} vs. low- \bar{A} experiment (Fig. 8A). The second point might seem to be inconsistent with the observation that the trend in overbank D_{ST} as a function of mass-balance location does not vary strongly between experiments (Fig. 8A). However, we note that the difference in planform area of the two routing systems (Fig. 3) meant that there were a greater number of overbank sites far from a channel in the low- \bar{A} vs. high- \bar{A} experiment. This tilted the deposition rate distribution towards lower values in the low- \bar{A} vs. high- \bar{A} experiment.

One important observation regarding overbank sedimentation is that the far-field overbank D_{ST} was similar in the two experiments (Fig. 9). We note that this far-field overbank aggradation rate factors into the calculation for avulsion setup timescales (Eq. 1). However, given the nearly equivalent T_{ST}^* estimates between experiments in χ space (Fig. 12A), our results suggest that channels are more sensitive than floodplains to accommodation production rates because channels are where deposition rates vary just enough to cause avulsion and compensation timescales to co-vary proportionally in response to accommodation production. This might be due to the connection that many channels have with the shoreline, and thus baselevel through processes that induce non-uniform flow like the development of backwater (Lamb et al. 2012; Wu and Nitterour 2020), while deposition in far-field overbank sites lacks the regional influence of sea-level.

CONCLUSIONS

Using results from a suite of physical fan-delta experiments, we explore gradients in key autogenic timescales and preserved depositional environments in strata within a mass-balance framework. We focus on channelized systems that preserve a significant volume of sediment deposited from suspension fallout in overbank settings. All forcing parameters were identical in the two experiments, except for the production of accommodation by sea-level rise. This allowed us to explore the universality of observations made in mass-balance space from bedload-dominated fan-delta experiments (Strong et al. 2005; Paola and Martin 2012) and explore the role of accommodation production on stratigraphic architecture. We find:

1. Measurements of surface morphology, deposition rates, and channel mobility suggest that autogenic timescales inversely scale with accommodation production rates (Fig. 11).
2. Metrics that quantify ratios of the vertical mobility of a delta through deposition (compensation timescale) to the lateral mobility of a network (either avulsion-setup timescale or channel-visitation timescale) were independent of accommodation production rate when placed in a mass-balance space (Fig. 12). This self-organized response to accommodation production provides a process framework to explain the utility of balancing mass for prediction of stratigraphic properties.
3. Measured gradients in the fraction of strata composed of key depositional environments show good agreement between experiments when placed in mass-balance space (Fig. 14). This suggests that stratigraphic architecture is independent of accommodation production in a mass-balance framework. This is particularly true for depositional environments linked to bedload transport (channels and terminal lobes). We suggest that low terrestrial retention of fines overbanking channels near shorelines partially explains differences in overbank strata in our experiments. However, in field-scale studies that explore large source-to-sink sediment routing systems, the loss of fine overbanking sediment to the marine near shorelines might not be an important factor for prediction of overbank-strata volumetrics.
4. Trends in channel deposition rates are sensitive to accommodation production rates in our experiments. However, overbank deposition rates as a function of mass-balance space are relatively insensitive to accommodation production rates in our experiments (Fig. 8). Thus, most of the differences in autogenic timescales in our experiments are due to the sensitivity of channels to processes that generate accommodation.

SUPPLEMENTAL MATERIAL

Data from the low and high accommodation production experiments (TDB-17-1 and TDB-18-1, respectively) are accessible through the Sustainable Environment–Actionable Data (SEAD) project data repository in collaboration with the Sediment Experimentalist Network. All data can be accessed through the Tulane Sediment Dynamics and Quantitative

Stratigraphy Group's collection at <https://sead2.ncsa.illinois.edu/collection/596d28c5e4b05e3417b2096f>.

ACKNOWLEDGMENTS

This study was supported by the National Science Foundation (grants EAR-1424312 and EAR-1848994). We thank Akinbobola Akintomide for his help completing the low-accommodation-production experiment. We also thank Elizabeth Hajek, an anonymous reviewer, and associate editor Elisabeth Steel for constructive suggestions that improved the manuscript.

REFERENCES

- ALLEN, J.R.L., 1978, Studies in fluvial sedimentation: an exploratory quantitative model for the architecture of avulsion-controlled alluvial sites: *Sedimentary Geology*, v. 26, p. 617–644.
- BAREFOOT, E.A., NITTROUER, J.A., AND STRAUB, K.M., 2021, Non-monotonic floodplain responses to changes in flooding intensity: *Journal of Geophysical Research: Earth Surface*, v. 126, p. e2021JF006310.
- BRIDGE, J.S., AND LEEDER, M.R., 1979, A simulation model of alluvial stratigraphy: *Sedimentology*, v. 26, p. 617–644.
- BRISTOW, C., AND BEST, J.L., 1993, Braided rivers: perspectives and problems, *in* Bristow, C., and Best, J.L., eds., *Braided Rivers*: Geological Society of London, Special Publication 75, p. 1–11.
- BRYANT, M., FALK, P., AND PAOLA, C., 1995, Experimental-study of avulsion frequency and rate of deposition: *Geology*, v. 23, p. 365–368.
- CALDWELL, R.L., AND EDMONDS, D.A., 2014, The effects of sediment properties on deltaic processes and morphologies: a numerical modeling study: *Journal of Geophysical Research, Earth Surface*, v. 119, p. 961–982.
- CAZANACLI, D., PAOLA, C., AND PARKER, G., 2002, Experimental steep, braided flow: application to flooding risk on fans: *Journal of Hydraulic Engineering*, v. 128, p. 322–330.
- CHADWICK, A.J., LAMB, M.P., AND GANTI, V., 2020, Accelerated river avulsion frequency on lowland deltas due to sea-level rise: *National Academy of Sciences, Proceedings*, v. 117, p. 17,584–517,590.
- CHAMBERLIN, E.P., AND HAJEK, E.A., 2015, Interpreting paleo-avulsion dynamics from multistory sand bodies: *Journal of Sedimentary Research*, v. 85, p. 82–94.
- CHAMBERLIN, E.P., AND HAJEK, E.A., 2019, Using bar preservation to constrain reworking in channel-dominated fluvial stratigraphy: *Geology*, v. 47, p. 531–534.
- CHAMBERLIN, E.P., HAJEK, E.A., AND TRAMPUSH, S.M., 2016, Measuring scales of autogenic organization in fluvial stratigraphy: an example from the Cretaceous Lower Williams Fork Formation, Colorado, *in* Budd, D.A., Hajek, E.A., and Purkis, S.J., eds., *Autogenic Dynamics and Self-Organization in Sedimentary Systems*: SEPM, Special Publication 106, p. 132–144.
- COLOMBERA, L., MOUNTNEY, N.P., AND MCCAFFREY, W.D., 2015, A meta-study of relationships between fluvial channel-body stacking pattern and aggradation rate: implications for sequence stratigraphy: *Geology*, v. 43, p. 283–286.
- DAVID, S.R., CZUBA, J.A., EDMONDS, D.A., AND WARD, A.S., 2022, The influence of floodplain channel connectivity on flood hydrodynamics: *Authora Preprints*.
- EDMONDS, D.A., HOYAL, D.C.J.D., SHEETS, B.A., AND SLINGERLAND, R.L., 2009, Predicting delta avulsions: implications for coastal wetland restoration: *Geology*, v. 37, p. 759–762.
- ESPOSITO, C.R., DI LEONARDO, D., HARLAN, M., AND STRAUB, K.M., 2018, Sediment storage partitioning in alluvial stratigraphy: the influence of discharge variability: *Journal of Sedimentary Research*, v. 88, p. 717–726.
- FERGUSON, R.I., AND CHURCH, M., 2004, A simple universal equation for grain settling velocity: *Journal of Sedimentary Research*, v. 74, p. 933–937.
- FIELDING, C.R., TRUEMAN, J.D., AND ALEXANDER, J., 2006, Holocene depositional history of the Burdekin River Delta of northeastern Australia: a model for a low-accommodation, highstand delta: *Journal of Sedimentary Research*, v. 76, p. 411–428.
- GANTI, V., LAMB, M.P., AND MCELROY, B., 2014, Quantitative bounds on morphodynamics and implications for reading the sedimentary record: *Nature Communications*, v. 5, p. 3298.
- GANTI, V., LAMB, M.P., AND CHADWICK, A.J., 2019, Autogenic erosional surfaces in fluvio-deltaic stratigraphy from floods, avulsions, and backwater hydrodynamics: *Journal of Sedimentary Research*, v. 89, p. 815–832.
- GOODBRED, S.L., AND KUEHL, S.A., 1998, Floodplain processes in the Bengal Basin and the storage of Ganges–Brahmaputra river sediment: an accretion study using ^{137}Cs and ^{210}Pb geochronology: *Sedimentary Geology*, v. 121, p. 239–258.
- HAJEK, E.A., 2009, Characterizing and interpreting channel-body clustering in the Ferris Formation, Hanna Basin, Wyoming [Ph.D. Thesis]: University of Wyoming, 211 p.
- HAJEK, E.A., AND STRAUB, K.M., 2017, Autogenic sedimentation in clastic stratigraphy: *Annual Review of Earth and Planetary Sciences*, v. 45, p. 681–709.
- HAJEK, E.A., AND WOLINSKY, M.A., 2012, Simplified process modeling of river avulsion and alluvial architecture: connecting models and field data: *Sedimentary Geology*, v. 257, p. 1–30.
- HAJEK, E.A., HELLER, P.L., AND SHEETS, B.A., 2010, Significance of channel-belt clustering in alluvial basins: *Geology*, v. 38, p. 535–538.
- HAMPSON, G.J., DULLER, R.A., PETTER, A.L., ROBINSON, R.A., AND ALLEN, P.A., 2014, Mass-balance constraints on stratigraphic interpretation of linked alluvial–coastal–shelfal deposits from source to sink: example from Cretaceous Western Interior Basin, Utah and Colorado, U.S.A.: *Journal of Sedimentary Research*, v. 84, p. 935–960.
- HAN, J., AND KIM, W., 2022, Linking levee-building processes with channel avulsion: geomorphic analysis for assessing avulsion frequency and channel reoccupation: *Earth Surface Dynamics*, v. 10, p. 743–759.
- HARIHARAN, J., XU, Z., MICHAEL, H.A., PAOLA, C., STEEL, E., AND PASSALACQUA, P., 2021, Linking the surface and subsurface in river deltas, part 1: relating surface and subsurface geometries: *Water Resources Research*, v. 57, p. e2020WR029282.
- HELLER, P.L., AND PAOLA, C., 1996, Downstream changes in alluvial architecture: an exploration of controls on channel-stacking patterns: *Journal of Sedimentary Research*, v. 66, p. 297–306.
- HICKSON, T.A., SHEETS, B.A., PAOLA, C., AND KELBERER, M., 2005, Experimental test of tectonic controls on three-dimensional alluvial facies architecture: *Journal of Sedimentary Research*, v. 75, p. 710–722.
- HOYAL, D.C.J.D., AND SHEETS, B.A., 2009, Morphodynamic evolution of experimental cohesive deltas: *Journal of Geophysical Research, Earth Surface*, v. 114, no. F02009.
- JASECHKO, S., SEYBOLD, H., PERRONE, D., FAN, Y., AND KIRCHNER, J.W., 2021, Widespread potential loss of streamflow into underlying aquifers across the USA: *Nature*, v. 591, p. 391–395.
- JEROLMACK, D.J., 2009, Conceptual framework for assessing the response of delta channel networks to Holocene sea-level rise: *Quaternary Science Reviews*, v. 28, p. 1786–1800.
- JEROLMACK, D.J., AND MOHRIG, D., 2007, Conditions for branching in depositional rivers: *Geology*, v. 35, p. 463–466.
- JEROLMACK, D.J., AND PAOLA, C., 2007, Complexity in a cellular model of river avulsion: *Geomorphology*, v. 91, p. 259–270.
- JERVEY, M.T., 1988, Quantitative geological modeling of siliciclastic rock sequences and their seismic expression, *in* Wilgus, C.K., Hastings, B.S., Kendall, C.G.S.C., Posamentier, H.W., Ross, C.A., and Van Wagoner, J.C., eds., *Sea Level Changes: An Integrated Approach*: SEPM, Special Publication 42, p. 47–69.
- KIM, W., MOHRIG, D., TWILLEY, R., PAOLA, C., AND PARKER, G., 2009, Is it feasible to build new land in the Mississippi River Delta?: *American Geophysical Union, EOS, Transactions*, v. 90, p. 373–374.
- KIM, W., SHEETS, B., AND PAOLA, C., 2010, Steering of experimental channels by lateral basin tilting: *Basin Research*, v. 22, p. 286–301.
- KLEINHANS, M.G., VAN DIJK, W.M., VAN DE LAGEWEG, W.I., HOYAL, D.C., MARKIES, H., VAN MAARSEVEEN, M., ROOSEDAAL, C., VAN WEESEER, W., VAN BREEMEN, D., AND HOENDERVOOGT, R., 2014, Quantifiable effectiveness of experimental scaling of river and delta morphodynamics and stratigraphy: *Earth-Science Reviews*, v. 133, p. 43–61.
- KRAUS, M.J., 2002, Basin-scale changes in floodplain paleosols: implications for interpreting alluvial architecture: *Journal of Sedimentary Research*, v. 72, p. 500–509.
- LAMB, M.P., NITTROUER, J.A., MOHRIG, D., AND SHAW, J., 2012, Backwater and river plume controls on scour upstream of river mouths: implications for fluvio-deltaic morphodynamics: *Journal of Geophysical Research: Earth Surface*, v. 117, p. F1.
- LAMB, M.P., DE LEEUW, J., FISCHER, W.W., MOODIE, A.J., VENDITTI, J.G., NITTROUER, J.A., HAUGHT, D., AND PARKER, G., 2020, Mud in rivers transported as flocculated and suspended bed material: *Nature Geoscience*, v. 13, p. 566–570.
- LEEDER, M.R., 1978, A quantitative stratigraphic model for alluvium, with special reference to channel deposit density and interconnectedness, *in* Miall, A.D., ed., *Fluvial Sedimentology*: Canadian Society of Petroleum Geologists, Memoir 5, p. 587–596.
- LI, Q., MATTHEW BENSON, W., HARLAN, M., ROBICHAUX, P., SHA, X., XU, K., AND STRAUB, K. M., 2017, Influence of sediment cohesion on deltaic morphodynamics and stratigraphy over basin-filling time scales: *Journal of Geophysical Research, Earth Surface*, v. 122, p. 1808–1826.
- MARTIN, H.K., AND EDMONDS, D.A., 2021, The push and pull of abandoned channels: how floodplain processes and healing affect avulsion dynamics and alluvial landscape evolution in foreland basins: *Earth Surface Dynamics, Discussions*, p. 1–42.
- MARTIN, J., SHEETS, B., PAOLA, C., AND HOYAL, D., 2009, Influence of steady base-level rise on channel mobility, shoreline migration, and scaling properties of a cohesive experimental delta: *Journal of Geophysical Research, Earth Surface*, v. 114, p. F3.
- MOHRIG, D., HELLER, P.L., PAOLA, C., AND LYONS, W.J., 2000, Interpreting avulsion process from ancient alluvial sequences: Guadalupe–Mataranya (northern Spain) and Wasatch Formation (western Colorado): *Geological Society of America, Bulletin*, v. 112, p. 1787–1803.
- MUTO, T., AND STEEL, R.J., 1997, Principles of regression and transgression: the nature of the interplay between accommodation and sediment supply: *Journal of Sedimentary Research*, v. 67, p. 994–1000.
- MUTO, T., AND STEEL, R.J., 2000, The accommodation concept in sequence stratigraphy: some dimensional problems and possible redefinition: *Sedimentary Geology*, v. 130, p. 1–10.
- MUTO, T., AND SWENSON, J.B., 2006, Autogenic attainment of large-scale alluvial grade with steady sea-level fall: an analog tank-flume experiment: *Geology*, v. 34, p. 161–164.
- NITTROUER, J.A., MOHRIG, D., AND ALLISON, M., 2011, Punctuated sand transport in the lowermost Mississippi River: *Journal of Geophysical Research, Earth Surface*, v. 116, p. F04025.
- NITTROUER, J.A., SHAW, J., LAMB, M.P., AND MOHRIG, D., 2012, Spatial and temporal trends for water-flow velocity and bed-material sediment transport in the lower Mississippi River: *Geological Society of America, Bulletin*, v. 124, p. 400–414.
- PAOLA, C., AND MARTIN, J.M., 2012, Mass-balance effects in depositional systems: *Journal of Sedimentary Research*, v. 82, p. 435–450.

- PAOLA, C., MULLIN, J., ELLIS, C., MOHRIG, D., SWENSON, J.B., PARKER, G., HICKSON, T., HELLER, P.L., PRATSON, L., SYVITSKI, J.P.M., SHEETS, B., AND STRONG, N., 2001, Experimental stratigraphy: *GSA Today*, v. 1, p. 4–9.
- PAOLA, C., STRAUB, K., MOHRIG, D., AND REINHARDT, L., 2009, The “unreasonable effectiveness” of stratigraphic and geomorphic experiments: *Earth-Science Reviews*, v. 97, p. 1–43.
- PARKER, G., PAOLA, C., WHIPPLE, K.X., AND MOHRIG, D., 1998, Alluvial fans formed by channelized fluvial and sheet flow. I: Theory: *Journal of Hydraulic Engineering*, v. 124, p. 985–995.
- PISEL, J.R., PYLES, D.R., AND KIRSCHBAUM, M.A., 2018, The influence of lateral topographic confinement on fluvial channel-belt clustering, compensation and connectivity: lower Wasatch Formation and Dakota Sandstone, Utah, USA: *Sedimentology*, v. 65, p. 597–619.
- PIZZUTO, J.E., 1987, Sediment diffusion during overbank flows: *Sedimentology*, v. 34, p. 301–317.
- PIZZUTO, J.E., MOODY, J.A., AND MEADE, R.H., 2008, Anatomy and dynamics of a floodplain, Powder River, Montana, U.S.A.: *Journal of Sedimentary Research*, v. 78, p. 16–28.
- PLINK-BIÖRKLUND, P., 2015, Morphodynamics of rivers strongly affected by monsoon precipitation: review of depositional style and forcing factors: *Sedimentary Geology*, v. 323, p. 110–147.
- POWELL, E.J., KIM, W., AND MUTO, T., 2012, Varying discharge controls on timescales of autogenic storage and release processes in fluvio-deltaic environments: tank experiments: *Journal of Geophysical Research: Earth Surface*, v. 117, p. F02011.
- SADLER, P.M., 1981, Sediment accumulation rates and the completeness of stratigraphic sections: *Journal of Geology*, v. 89, p. 569–584.
- SAHOO, H., GANI, M.R., GANI, N.D., HAMPSON, G.J., HOWELL, J.A., STORMS, J.E., MARTINIUS, A.W., AND BUCKLEY, S.J., 2020, Predictable patterns in stacking and distribution of channelized fluvial sand bodies linked to channel mobility and avulsion processes: *Geology*, v. 48, p. 903–907.
- SCHUMER, R., AND JEROLMACK, D.J., 2009, Real and apparent changes in sediment deposition rates through time: *Journal of Geophysical Research, Earth Surface*, v. 114, p. F00a06.
- SHEETS, B.A., HICKSON, T.A., AND PAOLA, C., 2002, Assembling the stratigraphic record: depositional patterns and time-scales in an experimental alluvial basin: *Basin Research*, v. 14, p. 287–301.
- SINCAVAGE, R., PAOLA, C., AND GOOBBRED, S., 2019, Coupling mass extraction and downstream fining with fluvial facies changes across the Sylhet basin of the Ganges–Brahmaputra–Meghna delta: *Journal of Geophysical Research: Earth Surface*, v. 124, p. 400–413.
- STRAUB, K.M., AND ESPOSITO, C.R., 2013, Influence of water and sediment supply on the stratigraphic record of alluvial fans and deltas: process controls on stratigraphic completeness: *Journal of Geophysical Research: Earth Surface*, v. 118, p. 1–13.
- STRAUB, K.M., AND WANG, Y., 2013, Influence of water and sediment supply on the long-term evolution of alluvial fans and deltas: statistical characterization of basin-filling sedimentation patterns: *Journal of Geophysical Research: Earth Surface*, v. 118, p. 1–15.
- STRAUB, K.M., PAOLA, C., MOHRIG, D., WOLINSKY, M.A., AND GEORGE, T., 2009, Compensational stacking of channelized sedimentary deposits: *Journal of Sedimentary Research*, v. 79, p. 673–688.
- STRAUB, K.M., LI, Q., AND BENSON, W.M., 2015, Influence of sediment cohesion on deltaic shoreline dynamics and bulk sediment retention: a laboratory study: *Geophysical Research Letters*, v. 42, p. 9808–9815.
- STRAUB, K.M., DULLER, R.A., FOREMAN, B.Z., AND HAJEK, E.A., 2020, Buffered, incomplete, and shredded: the challenges of reading an imperfect stratigraphic record: *Journal of Geophysical Research, Earth Surface*, v. 125, p. e2019JF005079.
- STRONG, N., AND PAOLA, C., 2008, Valleys that never were: time surfaces versus stratigraphic surfaces: *Journal of Sedimentary Research*, v. 78, p. 579–593.
- STRONG, N., SHEETS, B.A., HICKSON, T.A., AND PAOLA, C., 2005, A mass-balance framework for quantifying downstream changes in fluvial architecture, *in* Blum, M., Marriott, S., and Leclair, S., eds., *Fluvial Sedimentology VII: International Association of Sedimentologists, Special Publication 35*, p. 243–253.
- SUTFIN, N.A., WOHL, E.E., AND DWIRE, K.A., 2016, Banking carbon: a review of organic carbon storage and physical factors influencing retention in floodplains and riparian ecosystems: *Earth Surface Processes and Landforms*, v. 41, p. 38–60.
- TOONEN, W.H., FOULDS, S.A., MACKLIN, M.G., AND LEWIN, J., 2017, Events, episodes, and phases: signal from noise in flood-sediment archives: *Geology*, v. 45, p. 331–334.
- TORNOQVIST, T.E., 1993, Holocene alternation of meandering and anastomosing fluvial systems in the Rhine–Meuse delta (central Netherlands) controlled by sea-level rise and subsoil erodibility: *Journal of Sedimentary Research*, v. 63, p. 683–693.
- TRAMPUSH, S., HAJEK, E., STRAUB, K., AND CHAMBERLIN, E., 2017, Identifying autogenic sedimentation in fluvial-deltaic stratigraphy: evaluating the effect of outcrop-quality data on the compensation statistic: *Journal of Geophysical Research: Earth Surface*, v. 122, p. 1–23.
- WANG, Y., STRAUB, K.M., AND HAJEK, E.A., 2011, Scale-dependent compensational stacking: an estimate of autogenic time scales in channelized sedimentary deposits: *Geology*, v. 39, p. 811–814.
- WANG, Y., STORMS, J.E., MARTINIUS, A.W., KARSENBERG, D., AND ABELS, H.A., 2021, Evaluating alluvial stratigraphic response to cyclic and non-cyclic upstream forcing through process-based alluvial architecture modelling: *Basin Research*, v. 33, p. 48–65.
- WEISSMANN, G.S., HARTLEY, A.J., NICHOLS, G.J., SCUDERI, L.A., OLSON, M., BUEHLER, H., AND BANTEAH, R., 2010, Fluvial form in modern continental sedimentary basins: distributive fluvial systems: *Geology*, v. 38, p. 39–42.
- WHIPPLE, K.X., PARKER, G., PAOLA, C., AND MOHRIG, D., 1998, Channel dynamics, sediment transport, and the slope of alluvial fans: experimental study: *Journal of Geology*, v. 106, p. 677–693.
- WICKERT, A.D., MARTIN, J.M., TAL, M., KIM, W., SHEETS, B., AND PAOLA, C., 2013, River channel lateral mobility: metrics, time scales, and controls: *Journal of Geophysical Research Earth Surface*, v. 118, doi:10.1029/2012JF002386.
- WILLIAMS, G.P., 1978, Bank-full discharge of rivers: *Water Resources Research*, v. 14, p. 1141–1154.
- WINTER, T.C., 1999, Relation of streams, lakes, and wetlands to groundwater flow systems: *Hydrogeology Journal*, v. 7, p. 28–45.
- WOOD, L.J., ETHRIDGE, F.G., AND SCHUMM, S.A., 1993, The effects of rate of base-level fluctuation on coastal-plain, shelf and slope depositional systems: an experimental approach, *in* Posamentier, H.W., Summerhayes, C.P., Haq, B.U., and Allen, G.P., eds., *Sequence Stratigraphy and Facies Associations: International Association of Sedimentologists*, p. 43–53.
- WU, C., AND NITTRouer, J.A., 2020, Impacts of backwater hydrodynamics on fluvial-deltaic stratigraphy: *Basin Research*, v. 32, p. 567–584.

Received 20 December 2022; accepted 19 July 2023.